

Tetrahedral shapes of neutron-rich Zr isotopes from multidimensionally-constrained relativistic Hartree-Bogoliubov model

Jie Zhao (赵杰),^{1,2} Bing-Nan Lu (吕炳楠),^{1,3} En-Guang Zhao (赵恩广),^{1,4} and Shan-Gui Zhou (周善贵)^{1,5,4,6,*}

¹*CAS Key Laboratory of Theoretical Physics, Institute of Theoretical Physics, Chinese Academy of Sciences, Beijing 100190, China*

²*Physics Department, Faculty of Science, University of Zagreb, Bijenicka 32, Zagreb 10000, Croatia*

³*Institut für Kernphysik (IKP-3) and Jülich Center for Hadron Physics, Forschungszentrum Jülich, D-52425 Jülich, Germany*

⁴*Center of Theoretical Nuclear Physics, National Laboratory of Heavy Ion Accelerator, Lanzhou 730000, China*

⁵*School of Physics, University of Chinese Academy of Sciences, Beijing 100049, China*

⁶*Synergetic Innovation Center for Quantum Effects and Application, Hunan Normal University, Changsha, 410081, China*

(Dated: July 9, 2018)

We develop a multidimensionally constrained relativistic Hartree-Bogoliubov (MDC-RHB) model in which the pairing correlations are taken into account by making the Bogoliubov transformation. In this model, the nuclear shape is assumed to be invariant under the reversion of x and y axes; i.e., the intrinsic symmetry group is V_4 and all shape degrees of freedom $\beta_{\lambda\mu}$ with even μ are included self-consistently. The RHB equation is solved in an axially deformed harmonic oscillator basis. A separable pairing force of finite range is adopted in the MDC-RHB model. The potential energy curves of neutron-rich even-even Zr isotopes are calculated with relativistic functionals DD-PC1 and PC-PK1 and possible tetrahedral shapes in the ground and isomeric states are investigated. The ground state shape of ^{110}Zr is predicted to be tetrahedral with both functionals and so is that of ^{112}Zr with the functional DD-PC1. The tetrahedral ground states are caused by large energy gaps around $Z = 40$ and $N = 70$ when β_{32} deformation is included. Although the inclusion of the β_{30} deformation can also reduce the energy around $\beta_{20} = 0$ and lead to minima with pear-like shapes for nuclei around ^{110}Zr , these minima are unstable due to their shallowness.

PACS numbers: 21.60.Jz, 21.10.Dr, 27.60.+j

I. INTRODUCTION

The intrinsic shape of most known nuclei deviates from a sphere [1, 2]. The deformation of a nucleus can be described by the parametrization of the nuclear surface with a multipole expansion,

$$R(\theta, \varphi) = R_0 \left[1 + \beta_{00} + \sum_{\lambda=1}^{\infty} \sum_{\mu=-\lambda}^{\lambda} \beta_{\lambda\mu}^* Y_{\lambda\mu}(\theta, \varphi) \right], \quad (1)$$

where $\beta_{\lambda\mu}$'s are deformation parameters. Various nuclear deformations characterized by $\beta_{\lambda\mu}$ with different $\{\lambda, \mu\}$ are connected with many nuclear phenomena which have been predicted and some of them have also been observed.

In recent decades, the triaxiality and reflection asymmetry in nuclear shapes have become more and more attractive because several interesting theoretical predictions related to these shapes have been confirmed experimentally. The static triaxial shapes may result in the wobbling motion [2] or chiral doublet bands [3] in atomic nuclei; both phenomena were observed in 2001 [4, 5]. In 2006, Meng et al. predicted that multiple chiral doublet ($M\chi D$) bands may exist in one nucleus with different triaxial configurations [6]. In recent years, $M\chi D$

bands were indeed found in several nuclei [7–11]. The triaxiality may also play a role in the low-spin signature inversion [12–17]. Moreover, the development of triaxial shapes could lead to the termination of rotational bands in nuclei with $A \simeq 110$; see Ref. [18] for a review. The pear-like nuclear shape, characterized by β_{30} , was predicted to be very pronounced in many nuclei [19–21]. Low-lying negative-parity levels which are connected with the ground state band via strong $E1$ transitions in actinides and some rare-earth nuclei are related to reflection asymmetric shapes with nonzero β_{30} [22–31]. The direct evidence for a static octupole deformation has been shown experimentally in ^{224}Ra [32] and in ^{144}Ba [33].

What new features can we expect if the nonaxial and reflection asymmetric deformations are put together or combined? It has been revealed in Ref. [34] that both the triaxial and octupole shapes become important around the second saddle point in the potential energy surface (PES) of actinide nuclei and they lower the second fission barrier considerably. Recently, Liu et al. observed for the first time octupole correlations between $M\chi D$ bands in ^{78}Br and proposed that chirality-parity quartet bands may appear in a nucleus with both a static triaxial deformation (β_{22}) and an octupole deformation (β_{30}) [11].

The nonaxiality and reflection asymmetry are combined intrinsically in deformations characterized by $\beta_{\lambda\mu}$ with odd λ and nonzero μ . Among such deformations, the β_{32} deformation is of particular interest and has been investigated extensively [35–44]. A nucleus with

* sgzhou@itp.ac.cn

a pure β_{32} deformation, i.e., $\beta_{\lambda\mu} = 0$ if $\lambda \neq 3$ and $\mu \neq 2$, has a tetrahedral shape with the symmetry group T_d^D . The study of single-particle structure of a nucleus with tetrahedral symmetry predicted large energy gaps at $Z(N) = 16, 20, 32, 40, 56\text{--}58, 70$, and $90\text{--}94$ and $N = 112$ and $136/142$ [37, 40, 45–48]. These shell gaps are comparable to or even stronger than those at spherical shapes. Thus, a nucleus with proton and/or neutron numbers equal to these values may have a static tetrahedral shape or strong tetrahedral correlations.

Various nuclei such as $^{80,108,110}\text{Zr}$, ^{160}Yb , ^{156}Gd , and ^{242}Fm were predicted to have ground or isomeric states with tetrahedral shapes from the macroscopic-microscopic (MM) model [40, 41, 45, 49, 50] and the Skyrme Hartree-Fock (SHF) model, the SHF plus BCS model, or the Skyrme Hartree-Fock-Bogoliubov (SHFB) model [38, 39, 41–43, 45, 49, 51]. The possible existence of tetrahedral symmetry in light nuclei such as ^{16}O [52] as well as superheavy nuclei [53, 54] was also proposed. Furthermore, the rotational properties of tetrahedral nuclei have been studied theoretically [55–57] which would certainly be helpful for experimentalists to identify tetrahedral nuclei.

Several experiments were devoted to the study of tetrahedral shapes in ^{160}Yb [58], $^{154,156}\text{Gd}$ [58–60], $^{230,232}\text{U}$ [61], and ^{108}Zr [62]. For ^{160}Yb and $^{154,156}\text{Gd}$, although the observed odd and even-spin members of the lowest energy negative-parity bands are similar to the proposed tetrahedral band of ^{156}Gd , the deduced nonzero quadrupole moments existence of tetrahedral shapes in these nuclei. The possibility of a tetrahedral shape for the negative-parity bands in $^{230,232}\text{U}$ was excluded in Ref. [61] by the observed similarity in the energies and electric dipole moments of those bands in the $N = 138$ and $N = 140$ isotones and the measured values for quadrupole moment Q_2 in ^{226}Ra . An isomeric state observed in ^{108}Zr has been assigned a tetrahedral shape [62]. However, this isomeric state can also be explained by assuming an axial shape with the angular momentum projected shell model [63, 64].

Besides the tetrahedral shape which corresponds to a pure β_{32} deformation, the study of nuclear shapes with a non-zero β_{32} superposed on a sizable β_{20} has become a hot topic too. In recent years, nuclei with $Z \simeq 100$ have been studied extensively because such studies can not only reveal the structure for these nuclei but also give useful structure information for superheavy nuclei [65–78]. One example of such studies is the observation of very low-lying 2^- bands in several even- Z $N = 150$ isotones [79]. This low-lying feature was argued by Chen et al. to be a fingerprint of sizable β_{32} in these well deformed nuclei [80]. A self-consistent and microscopic study of Y_{32} effects in these $N = 150$ isotones was carried out in Ref. [81] and it was found that, for ground states of ^{248}Cf and ^{250}Fm , $\beta_{32} > 0.03$ and the energy gain due to the β_{32} distortion is more than 300 keV.

In this work we will study the potential energy surface and tetrahedral shape in neutron rich even-even Zr

isotopes by using the covariant density function theory (CDFT). The nuclear CDFT is one of the state-of-the-art approaches for the study of ground states as well as excited states in nuclei ranging from light to superheavy regions [82–92]. Recently, the global performance of various relativistic functionals on the ground state properties and beyond-mean-field correlations of nuclei across the nuclear chart has also been examined [76, 93–96].

Recently, we have developed multidimensionally constrained CDFT (MDC-CDFT) by breaking the reflection and axial symmetries simultaneously. In the MDC-CDFT, the nuclear shape is assumed to be invariant under the reversion of x and y axes; i.e., the intrinsic symmetry group is V_4 and all shape degrees of freedom $\beta_{\lambda\mu}$ with even μ ($\beta_{20}, \beta_{22}, \beta_{30}, \beta_{32}, \beta_{40}, \dots$) are included self-consistently. The MDC-CDFT consists of two types of models: the multidimensionally constrained relativistic mean field (MDC-RMF) model and the multidimensionally constrained relativistic Hartree-Bogoliubov (MDC-RHB) model. In the MDC-RMF model, the BCS approach has been implemented for the particle-particle (pp) channel. This model has been used to study potential energy surfaces and fission barriers of actinides [34, 97–101], the spontaneous fission of several fermium isotopes [102], the Y_{32} correlations in $N = 150$ isotones [81], and shapes of hypernuclei [103, 104]; see Refs. [105–107] for recent reviews. The Bogoliubov transformation generalizes the BCS quasi-particle concept and provides a unified description of particle-hole (ph) and pp correlations on a mean-field level. In the MDC-RHB model, pairing correlations are treated by making the Bogoliubov transformation and a separable pairing force of finite range [108–111] is adopted. Due to its finite range nature, the dependence of the results on the pairing cutoff can be avoided. The MDC-RHB model has been used to study the spontaneous fission of fermium isotopes [112].

The detailed formulas for the MDC-RMF model have been presented in Ref. [98] and some applications of this model were reviewed in Refs. [105–107]. In this paper, we present the formulas of the MDC-RHB model and its application to the study of tetrahedral shapes of neutron-rich Zr isotopes. The paper is organized as follows. The formalism of the MDC-RHB model is given in Sec. II. In Sec. III we present the numerical details and the results on neutron-rich even-even Zr isotopes. A summary is given in Sec. IV. Some detailed formulas used in the MDC-RHB model are given in Appendices A and B.

II. FORMALISM OF THE MDC-RHB MODEL

In the CDFT, a nucleus is treated as a system of nucleons interacting through exchanges of mesons and photons [82–92]. The effects of mesons are described either by mean fields or by point-like interactions between the nucleons [113, 114]. The nonlinear coupling terms [115–117] or the density dependence of the coupling constants [118, 119] were introduced to give correct satura-

tion properties of nuclear matter. Accordingly, there are four types of covariant density functionals: the meson exchange or point-coupling nucleon interactions combined with the nonlinear or density dependent couplings. All these four types of functionals have been implemented in the MDC-RHB model. In this section, we mainly present the formalism of the RHB model with density dependent point couplings.

The starting point of the RHB model with density dependent point couplings is the following Lagrangian,

$$\begin{aligned} \mathcal{L} = & \bar{\psi}(i\gamma_\mu\partial^\mu - M)\psi \\ & - \frac{1}{2}\alpha_S(\rho)\rho_S^2 - \frac{1}{2}\alpha_V(\rho)j_V^2 - \frac{1}{2}\alpha_{TV}(\rho)\vec{j}_{TV}^2 \\ & - \frac{1}{2}\delta_S(\partial_\nu\rho_S)(\partial^\nu\rho_S) \\ & - e\frac{1-\tau_3}{2}A_\mu j_V^\mu - \frac{1}{4}F^{\mu\nu}F_{\mu\nu}, \end{aligned} \quad (2)$$

where M is the nucleon mass, $\alpha_S(\rho)$, $\alpha_V(\rho)$, and $\alpha_{TV}(\rho)$ are density-dependent couplings for different channels, δ_S is the coupling constant of the derivative term, and e is the electric charge. ρ_S , j_V , and \vec{j}_{TV} are the isoscalar density, isoscalar current, and isovector current, respectively.

With the Green's function technique, one can derive the Dirac-Hartree-Bogoliubov equation [84, 120],

$$\int d^3\mathbf{r}' \begin{pmatrix} h - \lambda & \Delta \\ -\Delta^* & -h + \lambda \end{pmatrix} \begin{pmatrix} U_k \\ V_k \end{pmatrix} = E_k \begin{pmatrix} U_k \\ V_k \end{pmatrix}, \quad (3)$$

where E_k is the quasiparticle energy, λ is the chemical potential, and \hat{h} is the single-particle Hamiltonian,

$$\hat{h} = \boldsymbol{\alpha} \cdot [\mathbf{p} - \mathbf{V}(\mathbf{r})] + \beta[M + S(\mathbf{r})] + V_0(\mathbf{r}) + \Sigma_R(\mathbf{r}), \quad (4)$$

with the scalar potential, vector potential, and rearrangement terms,

$$\begin{aligned} S &= \alpha_S(\rho)\rho_S + \delta_S\Delta\rho_S, \\ V^\mu &= \alpha_V(\rho)j_V^\mu + \alpha_{TV}(\rho)j_{TV}^\mu \cdot \vec{\tau} + e\frac{1-\tau_3}{2}A^\mu, \\ \Sigma_R &= \frac{1}{2}\frac{\partial\alpha_S}{\partial\rho}\rho_S^2 + \frac{1}{2}\frac{\partial\alpha_V}{\partial\rho}j_V^2 + \frac{1}{2}\frac{\partial\alpha_{TV}}{\partial\rho}\vec{j}_{TV}^2. \end{aligned} \quad (5)$$

As usual we assume that the states are invariant under the time-reversal operation, which means that, in the above equations, all the currents or time-odd components vanish. In this case the single-particle Hamiltonian (4) has the time-reversal symmetry. For convenience two vector densities are defined as the time-like components of the 4-currents j_V and j_{TV} ,

$$\rho_V(\mathbf{r}) = j_v^0(\mathbf{r}), \quad \rho_{TV}(\mathbf{r}) = j_{TV}^0(\mathbf{r}), \quad (6)$$

which are the only surviving components. The densities are related to U_k 's and V_k 's through

$$\rho_S(\mathbf{r}) = \sum_{k>0} V_k^\dagger(\mathbf{r})\gamma_0 V_k(\mathbf{r}),$$

$$\begin{aligned} \rho_V(\mathbf{r}) &= \sum_{k>0} V_k^\dagger(\mathbf{r})V_k(\mathbf{r}), \\ \rho_{TV}(\mathbf{r}) &= \sum_{k>0} V_k^\dagger(\mathbf{r})\tau_3 V_k(\mathbf{r}). \end{aligned} \quad (7)$$

In the above summations, the no-sea approximation is applied.

The pairing potential reads

$$\begin{aligned} \Delta_{p_1 p_2}(\mathbf{r}_1 \sigma_1, \mathbf{r}_2 \sigma_2) &= \int d^3\mathbf{r}'_1 d^3\mathbf{r}'_2 \sum_{\sigma'_1 \sigma'_2}^{p'_1 p'_2} \\ & V_{p_1 p_2, p'_1 p'_2}^{\text{PP}}(\mathbf{r}_1 \sigma_1, \mathbf{r}_2 \sigma_2, \mathbf{r}'_1 \sigma'_1, \mathbf{r}'_2 \sigma'_2) \\ & \times \kappa_{p'_1 p'_2}(\mathbf{r}'_1 \sigma'_1, \mathbf{r}'_2 \sigma'_2), \end{aligned} \quad (8)$$

where $p = f, g$ is used to represent the large and small components of the Dirac spinor. V^{PP} is the effective pairing interaction and $\kappa(\mathbf{r}_1 \sigma_1, \mathbf{r}_2 \sigma_2)$ is the pairing tensor,

$$\kappa_{\alpha\alpha'}(\mathbf{r}_1 \sigma_1, \mathbf{r}_2 \sigma_2) = \sum_{k>0} V_{\alpha k}^*(\mathbf{r}_1 \sigma_1) U_{\alpha' k}(\mathbf{r}_2 \sigma_2). \quad (9)$$

As is usually done in the RHB theory, only the large components of the spinors are used to build the pairing potential [121]. In practical calculations this means

$$\begin{aligned} \Delta_{ff}(\mathbf{r}_1 \sigma_1, \mathbf{r}_2 \sigma_2) &= \int d^3\mathbf{r}'_1 d^3\mathbf{r}'_2 \sum_{\sigma'_1 \sigma'_2} \\ & V_{ff, ff}^{\text{PP}}(\mathbf{r}_1 \sigma_1, \mathbf{r}_2 \sigma_2, \mathbf{r}'_1 \sigma'_1, \mathbf{r}'_2 \sigma'_2) \\ & \times \kappa_{ff}(\mathbf{r}'_1 \sigma'_1, \mathbf{r}'_2 \sigma'_2). \end{aligned} \quad (10)$$

The other components Δ_{fg} , Δ_{gf} , and Δ_{gg} are omitted.

In the pp channel, we use a separable pairing force of finite range [108–111],

$$\begin{aligned} V(\mathbf{r}_1 \sigma_1, \mathbf{r}_2 \sigma_2, \mathbf{r}'_1 \sigma'_1, \mathbf{r}'_2 \sigma'_2) &= -G\delta(\mathbf{R} - \mathbf{R}')P(r)P(r') \\ & \times \frac{1}{2}(1 - P_\sigma), \end{aligned} \quad (11)$$

where G is the pairing strength and $\mathbf{R} = (\mathbf{r}_1 + \mathbf{r}_2)/2$ and $\mathbf{r} = \mathbf{r}_1 - \mathbf{r}_2$ are the center-of-mass and relative coordinates, respectively. $P(\mathbf{r})$ denotes the Gaussian function,

$$P(\mathbf{r}) = (4\pi a^2)^{-3/2} e^{-r^2/4a^2}, \quad (12)$$

where a is the effective range of the pairing force. The two parameters $G = G_0 = 728 \text{ MeV}\cdot\text{fm}^3$ and $a = 0.644 \text{ fm}$ [109, 110] have been adjusted to reproduce the density dependence of the pairing gap of symmetric nuclear matter at the Fermi surface calculated with the Gogny force D1S. In the present work, the pairing strength G is fine-tuned to reproduce the pairing gaps of Zr isotopes as discussed in Sec. III A.

The RHB equation (3) is solved by expanding the large and small components of the spinors $U_k(\mathbf{r}\sigma)$ and $V_k(\mathbf{r}\sigma)$ in an axially deformed harmonic oscillator (ADHO) basis

[122],

$$\begin{aligned} U_k(\mathbf{r}\sigma) &= \left(\begin{array}{c} \sum_{\alpha} f_U^{k\alpha} \Phi_{\alpha}(\mathbf{r}\sigma) \\ \sum_{\alpha} g_U^{k\alpha} \Phi_{\alpha}(\mathbf{r}\sigma) \end{array} \right), \\ V_k(\mathbf{r}\sigma) &= \left(\begin{array}{c} \sum_{\alpha} f_V^{k\alpha} \Phi_{\alpha}(\mathbf{r}\sigma) \\ \sum_{\alpha} g_V^{k\alpha} \Phi_{\alpha}(\mathbf{r}\sigma) \end{array} \right), \end{aligned} \quad (13)$$

with

$$\Phi_{\alpha}(\mathbf{r}\sigma) = C_{\alpha} \phi_{n_z}(z) \phi_{n_r}^{m_l}(\rho) \frac{1}{\sqrt{2\pi}} e^{im_l \varphi} \chi_{m_s}(\sigma), \quad (14)$$

which are eigensolutions of the Schrödinger equation with an ADHO potential,

$$\left[-\frac{\hbar^2}{2M} \nabla^2 + V_B(\rho, z) \right] \Phi_{\alpha}(\mathbf{r}\sigma) = E_{\alpha} \Phi_{\alpha}(\mathbf{r}\sigma), \quad (15)$$

with

$$V_B(\rho, z) = \frac{1}{2} M (\omega_{\rho}^2 \rho^2 + \omega_z^2 z^2). \quad (16)$$

In Eq. (14), C_{α} is a constant introduced for convenience, $\alpha = \{n_z, n_r, m_l, m_s\}$ is the collection of quantum numbers, and ω_z and ω_{ρ} are the oscillator frequencies along and perpendicular to the symmetry (z) axis, respectively. The deformation of the basis β_B is defined through relations $\omega_z = \omega_0 \exp(-\sqrt{5/4\pi} \beta_B)$ and $\omega_{\rho} = \omega_0 \exp(\sqrt{5/16\pi} \beta_B)$, where $\omega_0 = (\omega_z \omega_{\rho}^2)^{1/3}$ is the frequency of the corresponding spherical oscillator. These bases are also eigenfunctions of the z component of the angular momentum j_z with eigenvalues $K_{\alpha} = m_l + m_s$. For such a basis state $\Phi_{\alpha}(\mathbf{r}\sigma)$ we can define a time-reversal state by $\Phi_{\bar{\alpha}}(\mathbf{r}\sigma) = \mathcal{T} \Phi_{\alpha}(\mathbf{r}\sigma)$, where $\mathcal{T} = i\sigma_y K$ is the time-reversal operator and K is the complex conjugation. It is easy to see that $\Phi_{\bar{\alpha}}(\mathbf{r}\sigma)$ is also an eigensolution of Eq. (15) with the same energy E_{α} , while the direction of the angular momentum is reversed, $K_{\bar{\alpha}} = -K_{\alpha}$. $\{\Phi_{\alpha}, \Phi_{\bar{\alpha}} | K_{\alpha} > 0\}$ forms a complete and discrete basis set in the space of two-component spinors.

In practical calculations, the ADHO basis is truncated as [98, 123],

$$[n_z/Q_z + (2n_{\rho} + |m_l|)/Q_{\rho}] \leq N_f, \quad (17)$$

for the large component of the Dirac spinor. N_f is a certain integer constant and $Q_z = \max(1, b_z/b_0)$ and $Q_{\rho} = \max(1, b_{\rho}/b_0)$ are constants calculated from the oscillator lengths $b_0 = 1/\sqrt{M\omega_0}$, $b_z = 1/\sqrt{M\omega_z}$, and $b_{\rho} = 1/\sqrt{M\omega_{\rho}}$. For the small component, the truncation is made up to $N_g = N_f + 1$ major shells in order to avoid spurious states [122]. The convergence of the results on N_f is discussed in Sec. III A.

The V_4 symmetry is imposed in the MDC-CDFT [107]; i.e., the nuclear potentials and densities are invariant under the following operations

$$\begin{aligned} \hat{S}_x \phi(x, y, z) &= \phi(-x, y, z), \\ \hat{S}_y \phi(x, y, z) &= \phi(x, -y, z), \\ \hat{S} \phi(x, y, z) &= \phi(-x, -y, z), \end{aligned} \quad (18)$$

where $\phi(x, y, z)$ represents nuclear potentials and densities. Thus, both axial symmetry and reflection symmetry are broken. Due to the V_4 symmetry, one can introduce a simplex operator $\hat{S} = ie^{-i\pi j_z}$ to block-diagonalize the RHB matrix. For a fermionic system, \hat{S} is a Hermitian operator and satisfies $\hat{S}^2 = 1$. The basis states are also eigenstates of \hat{S} with $\hat{S} \Phi_{\alpha} = (-1)^{K_{\alpha} - \frac{1}{2}} \Phi_{\alpha}$, which means that Φ_{α} with $K_{\alpha} = \frac{1}{2}, -\frac{3}{2}, \frac{5}{2}, -\frac{7}{2}, \dots$ span a subspace with $S = +1$, while their time-reversal states span the one with $S = -1$. Due to the time-reversal symmetry, the RHB matrix is block-diagonalized into two smaller ones denoted by the quantum number $S = \pm 1$, respectively. Furthermore, for a system with the time-reversal symmetry, it is only necessary to diagonalize the matrix with $S = +1$ and the other half is obtained by making the time reversal operation on Dirac spinors.

In the $S = +1$ subspace, solving the RHB equation (3) is equivalent to diagonalizing the matrix

$$\begin{pmatrix} \mathcal{A} - \lambda & \mathcal{B} \\ \mathcal{B}^{\dagger} & -\mathcal{A}^* + \lambda \end{pmatrix} \begin{pmatrix} \mathcal{U}_k \\ \mathcal{V}_k \end{pmatrix} = E_k \begin{pmatrix} \mathcal{U}_k \\ \mathcal{V}_k \end{pmatrix}, \quad (19)$$

where $\mathcal{U}_k = (\mathcal{U}_{k,\alpha})$ and $\mathcal{V}_k = (\mathcal{V}_{k,\bar{\alpha}})$ are column matrices, and

$$\mathcal{A}_{\alpha\alpha'} = \langle \alpha | h | \alpha' \rangle, \quad \mathcal{B}_{\alpha\bar{\alpha}'} = \langle \alpha | \Delta | \bar{\alpha}' \rangle, \quad (20)$$

are matrix elements of the single-particle Hamiltonian and the pairing field, where α and α' run over all the quantum numbers $\{n_z, n_r, m_l, m_s, p\}$ satisfying the truncation condition (17).

We expand the potentials $V(\mathbf{r})$ and $S(\mathbf{r})$ and the densities in Eq. (7) in terms of the Fourier series,

$$f(\rho, \varphi, z) = \sum_{\mu=-\infty}^{\infty} f_{\mu}(\rho, z) \frac{1}{\sqrt{2\pi}} \exp(i\mu\varphi). \quad (21)$$

By applying the symmetry conditions (18), it is easy to see that $f_{\mu} = f_{\mu}^* = f_{\bar{\mu}}$ and $V_n = 0$ for odd n . Thus the expansion in Eq. (21) can be simplified as

$$f(\rho, \varphi, z) = f_0(\rho, z) \frac{1}{\sqrt{2\pi}} + \sum_{n=1}^{\infty} f_n(\rho, z) \frac{1}{\sqrt{\pi}} \cos(2n\varphi), \quad (22)$$

where

$$\begin{aligned} f_0(\rho, z) &= \frac{1}{\sqrt{2\pi}} \int_0^{2\pi} d\varphi f(\rho, \varphi, z), \\ f_n(\rho, z) &= \frac{1}{\sqrt{\pi}} \int_0^{2\pi} d\varphi f(\rho, \varphi, z) \cos(2n\varphi), \end{aligned} \quad (23)$$

are real functions of ρ and z . The calculation of matrix elements $\mathcal{A}_{\alpha\alpha'}$ and densities are similar to that of the MDC-RMF model; the details can be found in Appendices of Ref. [98].

Due to the finite range nature of the pairing force given in Eq. (11), it is not easy to calculate the matrix element $V_{12,1'2'}^{PP}$, where the numbers 1, 2, 1', and 2' denote the ADHO basis wave functions. In Ref. [110], the authors

have shown that the anti-symmetrized matrix element $\bar{V}_{12,1'2'}^{PP} = V_{12,1'2'}^{PP} - V_{12,2'1'}^{PP}$ can be written as a sum of separable terms in both axially deformed and anisotropic HO bases. For this purpose the first step is to represent the product of two single-particle HO wave functions as a sum of HO wave functions in their center-of-mass frame,

$$|n_{r_1} m_1\rangle |n_{r_2} m_2\rangle = \sum_{N_p M_p} \sum_{n_p m_p} M_{N_p M_p n_p m_p}^{n_{r_1} m_1 n_{r_2} m_2} |N_p M_p\rangle |n_p m_p\rangle, \\ |n_{z_1}\rangle |n_{z_2}\rangle = \sum_{N_z n_z} M_{N_z n_z}^{n_{z_1} n_{z_2}} |N_z\rangle |n_z\rangle, \quad (24)$$

where $M_{N_z n_z}^{n_{z_1} n_{z_2}}$ and $M_{N_p M_p n_p m_p}^{n_{r_1} m_1 n_{r_2} m_2}$ are the Talmi-Moshinski brackets which are given in Appendix B. The matrix element in the center-of-mass frame reads

$$V_{12,1'2'} = -2\sqrt{2}G \sum_{N_z N_p M_p} \left(W_{12}^{N_z N_p M_p} \right)^* W_{1'2'}^{N_z N_p M_p} \quad (25)$$

where

$$W_{12}^{N_z N_p M_p} = \delta_{K_1+K_2, M_p} \delta_{\pi_1 \pi_2, (-1)^{N_z+|M_p|}} \tau_1 \frac{1}{\sqrt{2}} C_1 C_2 \\ \times \left(\sum_{n_z} M_{N_z n_z}^{n_{z_1} n_{z_2}} V_{n_z} \right) \\ \times \left(\sum_{n_p} M_{N_p M_p n_p 0}^{n_{r_1} m_1 n_{r_2} m_2} U_{n_p} \right), \quad (26)$$

and

$$V_{n_z} = \frac{1}{(4\pi a^2)^{1/2}} \int_{-\infty}^{\infty} dz e^{-\frac{z^2}{2a^2}} \phi_{n_z}(z), \\ U_{n_p} = \frac{\sqrt{2\pi}}{4\pi a^2} \int_0^{\infty} d\rho \rho e^{-\frac{\rho^2}{2a^2}} R_{n_p}^0(\rho). \quad (27)$$

More details are given in Appendix A. The pairing field and pairing energy can also be written in the separable form as

$$\Delta_{12} = \sum_{1'2'} V_{12,1'2'} \kappa_{1'2'} \\ = -2\sqrt{2}G \sum_{N_z} \sum_{N_p M_p} \left(W_{12}^{N_z N_p M_p} \right)^* P^{N_z N_p M_p} \quad (28) \\ E_{\text{pair}} = \frac{1}{2} \sum_{12,1'2'} V_{12,1'2'} \kappa_{12}^* \kappa_{1'2'} \\ = -\sqrt{2}G \sum_{N_z} \sum_{N_p M_p} |P^{N_z N_p M_p}|^2, \quad (29)$$

where

$$P^{N_z N_p M_p} = \sum_{12} W_{12}^{N_z N_p M_p} \kappa_{12}. \quad (30)$$

Since $\hat{S} = ie^{-i\pi j_z}$ is conserved, we can check that the matrix element of the pairing tensor has the structure $\kappa_{12} = \delta_{S_1, \bar{S}_2} \kappa_{12}$. Combined with the $\delta_{K_1+K_2, M_p}$ in $W_{12}^{N_z N_p M_p}$, one gets

$$P^{N_z N_p M_p} = \sum_{12} \delta_{S_1, \bar{S}_2} \delta_{K_1+K_2, M_p} W_{12}^{N_z N_p M_p} \kappa_{12}$$

$$= \delta_{M_p, 2n} P^{N_z N_p M_p}, \quad n \in Z, \quad (31)$$

i.e., only $P^{N_z N_p M_p}$ with even M_p survive and thus we can skip safely those with odd M_p in the sum in Eq. (28). The sum in Eq. (25) runs over the ADHO quantum numbers N_z , N_p , and M_p in the center-of-mass frame with $N_z + 2N_p + |M_p| \leq 2N_f$.

The total energy of the nucleus reads

$$E_{\text{total}} = \int d^3 \mathbf{r} \left\{ \sum_k v_k^2 \psi_k^\dagger (\boldsymbol{\alpha} \cdot \mathbf{p} + \beta M_B) \psi_k \right. \\ + \frac{1}{2} \alpha_S \rho_S^2 + \frac{1}{2} \alpha_V \rho_V^2 + \frac{1}{2} \alpha_{TS} \rho_{TS}^2 + \frac{1}{2} \alpha_{TV} \rho_{TV}^2 \\ + \frac{1}{3} \beta_S \rho_S^3 + \frac{1}{4} \gamma_S \rho_S^4 + \frac{1}{4} \gamma_V \rho_V^4 \\ + \frac{1}{2} \delta_S \rho_S \Delta \rho_S + \frac{1}{2} \delta_V \rho_V \Delta \rho_V \\ + \frac{1}{2} \delta_{TS} \rho_{TS} \Delta \rho_{TS} + \frac{1}{2} \delta_{TV} \rho_{TV} \Delta \rho_{TV} + \frac{1}{2} e \rho_C A \left. \right\} \\ + E_{\text{pair}} + E_{\text{c.m.}}, \quad (32)$$

where the center-of-mass correction $E_{\text{c.m.}}$ is calculated, depending on the relativistic functional, either phenomenologically as

$$E_{\text{c.m.}} = -\frac{3}{4} \times 41 A^{1/3} \text{ MeV}, \quad (33)$$

or from the quasiparticle vacuum

$$E_{\text{c.m.}} = -\frac{\langle P^2 \rangle}{2MA}, \quad (34)$$

where P is the total linear momentum and A is the nuclear mass number.

The intrinsic multipole moments are calculated as

$$Q_{\lambda\mu}^\tau = \int d^3 \mathbf{r} \rho_V^\tau(\mathbf{r}) r^\lambda Y_{\lambda\mu}(\Omega), \quad (35)$$

where $Y_{\lambda\mu}(\Omega)$ is the spherical harmonics and τ refers to the proton, neutron, or the whole nucleus. The deformation parameter $\beta_{\lambda\mu}$ is obtained from the corresponding multipole moment by

$$\beta_{\lambda\mu}^\tau = \frac{4\pi}{3N_\tau R^\lambda} Q_{\lambda\mu}^\tau, \quad (36)$$

where $R = 1.2 \times A^{1/3}$ fm and N_τ is the number of proton, neutron, or nucleons.

III. RESULTS AND DISCUSSIONS

In this section, we study neutron rich even-even Zr isotopes with $100 \leq A \leq 114$ by using the MDC-RHB model. These nuclei are among those with $N \simeq 70$ and $A \simeq 110$ which show interesting nuclear structure properties, such as drastic changes in shapes with A and shape

TABLE I. Pairing gaps (in MeV) calculated from functionals DD-PC1 [111] and PC-PK1 [166] for $^{102,104}\text{Zr}$. The experimental values are obtained from odd-even mass differences and the mass values are taken from Ref. [167].

	^{102}Zr		^{104}Zr	
	Δ_n	Δ_p	Δ_n	Δ_p
Experiment	1.10	1.55	1.08	1.55
DD-PC1	1.08	1.51	0.99	1.50
PC-PK1	1.17	1.60	1.11	1.60

coexistences [40, 42, 49, 51, 63, 64, 94, 124–141]. The structures of nuclei around $N = 70$ are also of particular interest for nuclear astrophysics because neutron-rich nuclei with $A \simeq 110$ are around the r -process path, which is determined by the equilibrium between neutron capture and photodisintegration [142–152].

Zr isotopes have been studied extensively with the CDFT under the assumption of reflection symmetry [94, 125, 127, 133, 135, 136, 139]. In these studies, the coexistence of prolate and oblate minima in potential energy curves of even-even Zr isotopes were discussed. By including the β_{30} deformation, a pear-like ground state of ^{112}Zr is predicted with the functional DD-PC1 [21]. From the experimental point of view, the analysis of rotational bands, β -decay half-lives, and lifetimes of the first 2^+ states reveals that some of these nuclei are well deformed [62, 152–164] and there exist shape coexistences in $^{100-104}\text{Zr}$ [153–155, 165].

Next we give some numerical details and illustrative calculations of the MDC-RHB model. Then we present and discuss the results for neutron-rich even-even Zr isotopes calculated with functionals DD-PC1 [111] and PC-PK1 [166].

A. Numerical details

In the MDC-RHB model, the potentials and densities are calculated in a spatial lattice in which mesh points in the ρ and z directions are designed in a way that the Gaussian quadrature can be performed and those for the azimuthal angle φ are equally distributed. Since we keep the mirror reflection symmetry with respect to the $x = 0$ or $y = 0$ planes, only mesh points with positive x and y are considered. For axially deformed nuclei the azimuthal degree of freedom vanishes, and for reflection symmetric nuclei mesh points with $z < 0$ can also be omitted. The values of the localized fields and potentials in the full lattice space can be simply obtained by symmetry transformations such as rotations or the spatial reflection.

To reproduce the available empirical pairing gaps of $^{102,104}\text{Zr}$ (see Table I), the strength of the pairing force given in Eq. (11) is readjusted a little for protons compared to those originally proposed in Refs. [109, 110]: $G_n = G_0$, $G_p = 1.12G_0$ with $G_0 = 738 \text{ MeV}\cdot\text{fm}^3$.

The calculated physical observables should converge

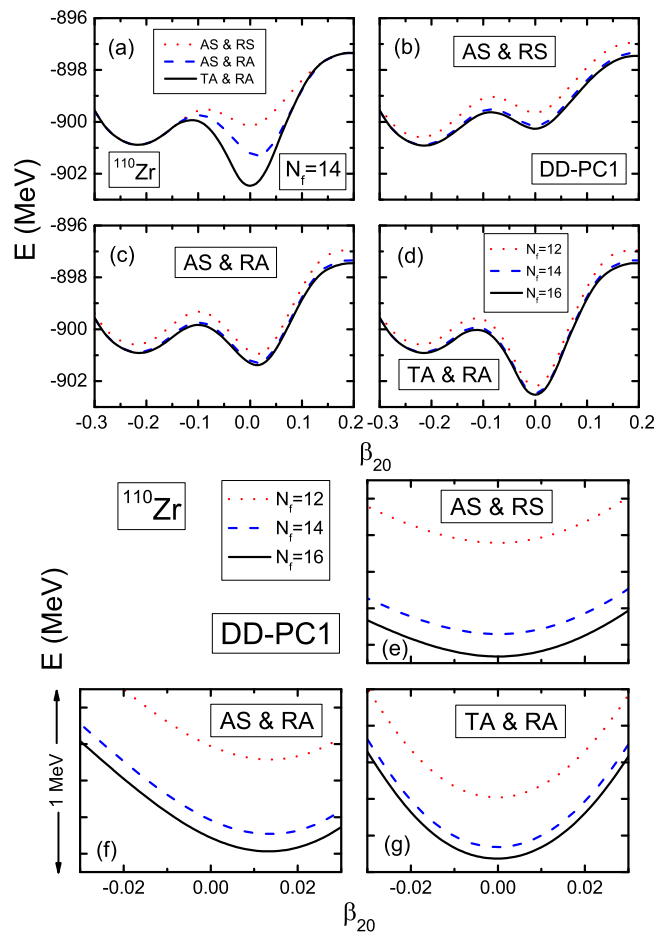


FIG. 1. (Color online) The potential energy curve of ^{110}Zr from MDC-RHB calculations with different symmetries imposed (a) and with different truncations of the ADHO basis [(b), (c), and (d)]. The calculations are performed with axial symmetry and reflection symmetry (AS & RS), axial symmetry and reflection asymmetry (AS & RA), and triaxial symmetry and reflection asymmetry (TA & RA) imposed, respectively. In [(b), (c), and (d)], the results calculated with $N_f = 12, 14,$ and 16 are depicted by dotted, dashed, and solid curves, respectively. The corresponding amplified figures [(e), (f), and (g)] show the detailed structure of the PES's near $\beta_{20} = 0$; the width of each subfigure is 0.06 and the height is 1 MeV .

as the truncation $N_f \rightarrow \infty$. In Fig. 1, we show the one-dimensional (1D) potential energy curve of ^{110}Zr around the ground state with axial symmetry and reflection symmetry, axial symmetry and reflection asymmetry, and nonaxial and reflection asymmetry imposed, respectively. The effective interaction DD-PC1 [111] is used. Calculations with different truncations ($N_f = 12, 14,$ and 16) are depicted by dotted, dashed, and solid curves, respectively. As shown in the upper panel of Fig. 1, the predicted ground state shape of ^{110}Zr is oblate with $\beta_{20} \approx -0.2$ when both axial and reflection symmetries are imposed. There is another minimum around $\beta_{20} = 0$. The energy of this minimum is reduced by about 1 MeV

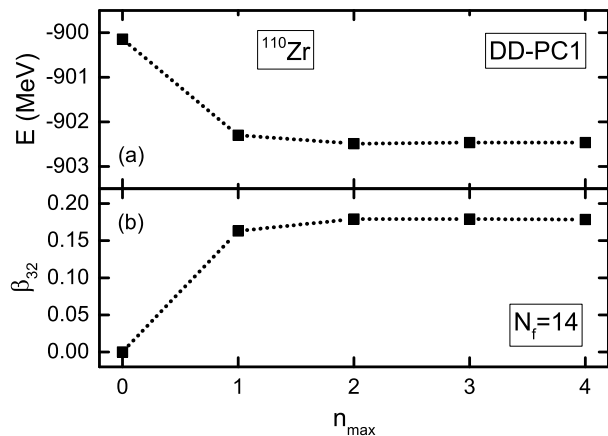


FIG. 2. The binding energy (a) and β_{32} deformation (b) of ^{110}Zr from MDC-RHB calculations with different truncations made in the Fourier expansion of densities and potentials. The calculations are performed with $N_f = 14$. The functional DD-PC1 is used in the MDC-RHB calculations.

when the axial octupole deformation (β_{30}) is included, while the energy gain is about 2 MeV when the nonaxial octupole deformation (β_{32}) is included. As a result, the ground state changes to be $\beta_{20} \approx 0$. To see more clearly the truncation errors, we have amplified the figure near $\beta_{20} = 0$. We can see that for ^{110}Zr , the energy changes about 400 keV when N_f increases from 12 to 14; further increasing N_f from 14 to 16, the energy changes only about 100 keV. Furthermore, from Fig. 1, one can find that the inaccuracy caused by the finite basis size is almost independent of the imposed symmetry (in this case, independent of whether the axial or nonaxial deformations, reflection symmetric or reflection asymmetric deformations are included). This means a good convergence and $N_f = 14$ is sufficient in this mass region.

For axially symmetric nuclei where potentials and densities $f(\rho, \varphi, z) \equiv f(\rho, z)$ are independent of the azimuthal angle φ , the Fourier coefficient $f_n(\rho, z) = 0$ when $n \geq 1$. For nonaxial nuclei, $f_n(\rho, z) \neq 0$ when $n \geq 1$. Therefore, n characterizes the nonaxiality of potentials and densities. In practical calculations, the Fourier series in Eq. (22) has to be truncated, i.e., $n \leq n_{\max}$. To study the dependence of the calculated results on n_{\max} , we show the binding energy and nonaxial β_{32} deformation parameter of ^{110}Zr calculated with different n_{\max} in Fig. 2. As shown in Fig. 2(b), if all f_n 's with $n \geq 1$ are omitted ($n_{\max} = 0$), the nucleus remains axial and $\beta_{32} = 0$. The convergence of the binding energy and β_{32} with n_{\max} increasing is very fast. The results obtained with $n_{\max} = 2$ are very precise already; the energy gain when n_{\max} increases from 2 to 3 is only around 30 keV. In practical calculations, n_{\max} is determined automatically by the relation $2n_{\max} = K_{\max} - K_{\min}$, where K_{\max} (K_{\min}) is the largest (smallest) K in the truncated ADHO basis. This is sufficiently large for all of results discussed here.

B. Neutron-rich even-even Zr isotopes

We calculate one-dimensional (1D) potential energy curves ($E \sim \beta_{20}$) for even-even Zr nuclei with $100 \leq A \leq 114$. The functionals DD-PC1 [111] and PC-PK1 [166] are used. To investigate different roles played by the non-axiality and reflection asymmetry, calculations are performed with different symmetries imposed: (i) axial and reflection symmetry, (ii) axial symmetry and reflection asymmetry, and (iii) nonaxial and reflection asymmetry, and the results are denoted by dotted, dash-dotted, and solid lines, respectively.

First we focus on 1D potential energy curves obtained with DD-PC1, which are shown in Fig. 3. If nuclear shapes are restricted to be axial and reflection symmetric (red dotted line), a prolate ground state with $\beta_{20} \approx 0.4$ coexisting with an oblate minimum with $\beta_{20} \approx -0.2$ is obtained for ^{100}Zr . This is consistent with the experimental observations [153, 154, 157, 158]. For $^{102-114}\text{Zr}$, the ground state shapes are predicted to be oblate with $\beta_{20} \approx -0.2$. As neutron number increases, the energy of the minimum with $\beta_{20} > 0$ increases. A minimum with $\beta_{20} \approx 0$ is developed starting from ^{106}Zr . This minimum becomes lower in energy and the pocket becomes deeper with the neutron number increasing.

If nuclei are allowed to be reflection asymmetric but axial symmetric, one obtains 1D potential energy curves, denoted by blue dash-dotted lines in Fig. 3. The β_{30} deformation is involved around $\beta_{20} = 0$ for all of the nuclei investigated here. As a result, a minimum develops for ^{104}Zr around $\beta_{20} = 0$. The energy of the minimum with $\beta_{20} \approx 0$ for $^{106-114}\text{Zr}$ is lowered substantially by the β_{30} distortion. Due to this lowering effect, the energy of the minimum with pear-like shape ($\beta_{20} \approx 0$, $\beta_{30} \neq 0$) is lower than the minimum with oblate or prolate shape for ^{110}Zr , ^{112}Zr , and ^{114}Zr . This lowering effect is also found in Skyrme HFB+BCS calculations [51]. The β_{30} deformation is not important either around the oblate minimum ($\beta_{20} \approx -0.2$) or around the prolate minimum ($\beta_{20} \approx 0.4$). Note that these results are different from those presented in Ref. [21] where the octupole deformation is found only in the ground state of ^{112}Zr with the functional DD-PC1. Such differences are mainly caused by different pairing strengths used in these two works. We have checked that if we use the pairing strengths given in Ref. [21], i.e., $G_n = G_p = 1.12G_0$ with $G_0 = 738 \text{ MeV}\cdot\text{fm}^3$, we can get the same results as Ref. [21].

When the β_{32} deformation is allowed in the calculations, both axial and reflection symmetries are broken. As seen in Fig. 3, the β_{32} deformation changes very much the energy around $\beta_{20} = 0$ (the black solid line). Similar to the cases discussed in the previous paragraph about the inclusion of β_{30} , a minimum also develops for ^{104}Zr around $\beta_{20} = 0$. However, the β_{32} distortion effect is more pronounced than that of the β_{30} deformation for most of these nuclei. The energy of the minimum with $\beta_{20} \approx 0$ for $^{106-112}\text{Zr}$ is lowered substantially. A tetrahedral ground state is predicted for $^{110,112}\text{Zr}$. For ^{114}Zr ,

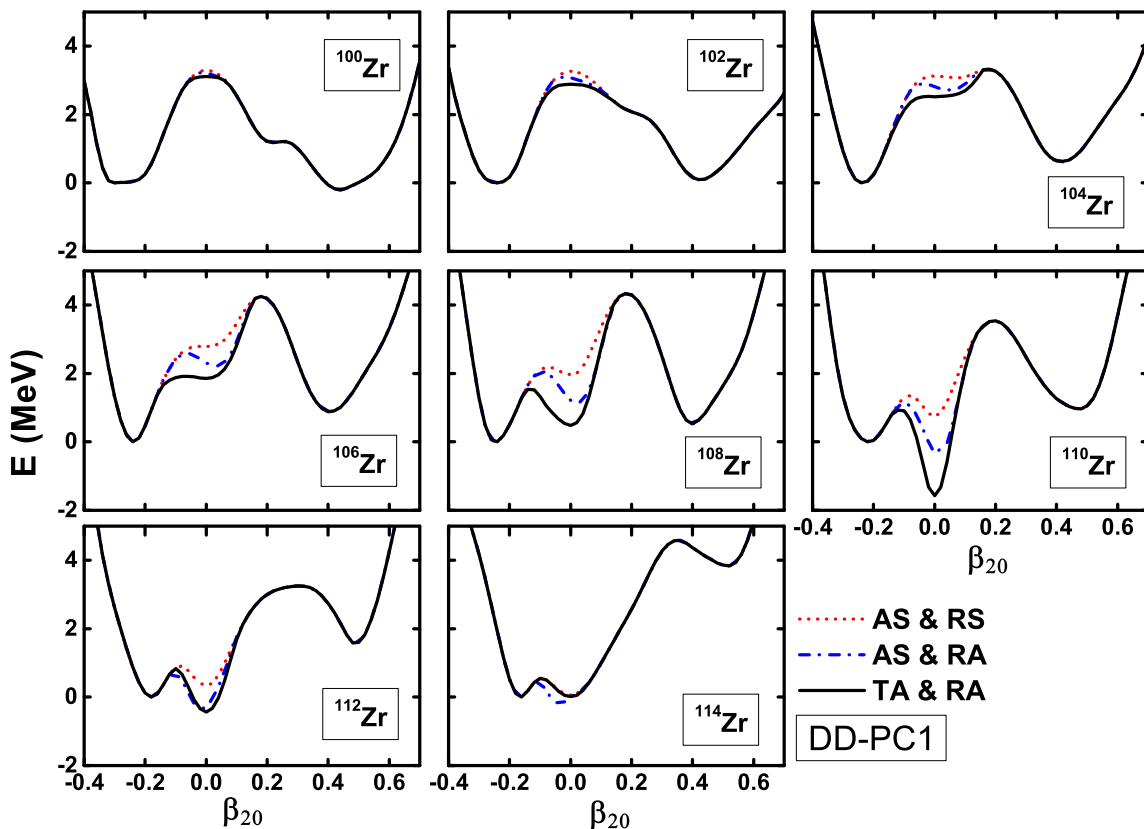


FIG. 3. (Color online) Potential energy curves ($E \sim \beta_{20}$) for Zr isotopes. The energy is normalized with respect to the energy minimum with $\beta_{20} < 0$ for each nucleus. The dotted line denotes results with axial symmetry (AS) and reflection symmetry (RS) imposed, the dash-dotted line denotes results restricted to AS and reflection asymmetry (RA), while the solid line represents results with both AS and RS broken, i.e., with triaxial (TA) deformation and RA. The functional DD-PC1 is used in MDC-RHB calculations.

the predicted pear-like shape is lower in energy than the tetrahedral shape. From Fig. 3, we know that the β_{32} distortion effect is the most pronounced for ^{110}Zr , where the inclusion of the β_{32} deformation lowers the energy of the minimum around $\beta_{20} = 0$ by about 2 MeV. Similar to the situation of β_{30} , the β_{32} deformation is important neither around the oblate minimum ($\beta_{20} \approx -0.2$) nor around the prolate minimum ($\beta_{20} \approx 0.4$). The obtained ground state deformation parameters as well as the binding energies with DD-PC1 for $^{110-114}\text{Zr}$ are listed in Table II. The corresponding available experimental values are also included for comparison. The predicted energies of various minima (with respect to the corresponding ground state energy) are presented in Table III.

From Fig. 3 and Table II, one finds that the ground states of $^{100-108}\text{Zr}$ are well deformed with large quadrupole deformation. For ^{108}Zr , a tetrahedral isomeric state is also predicted. The ground states of $^{110,112}\text{Zr}$ are predicted to have tetrahedral shape and the most pronounced effect from the β_{32} distortion is in ^{110}Zr with the functional DD-PC1. The formation of the tetrahedral ground state around ^{110}Zr can be traced back to the large energy gaps at $Z = 40$ and $N = 70$ in the single-particle levels when β_{32} deformation is in-

TABLE II. The quadrupole deformation β_{20} , axial octupole deformation β_{30} , nonaxial octupole deformation β_{32} , and hexadecapole deformation β_{40} together with binding energies E_{cal} for the ground states of Zr isotopes obtained in MDC-RHB calculations with the functional DD-PC1. E_{exp} denotes experimental binding energies taken from Ref. [167]. β_{exp} represents experimental quadrupole deformations taken from Ref. [168]. The data with “*” stand for estimated values [167]. All energies are in MeV.

Nucleus	β_{20}	β_{30}	β_{32}	β_{40}	E_{cal}	β_{exp}	E_{exp}
^{100}Zr	0.44	0.00	0.00	0.22	-851.90	0.36	-852.22
^{102}Zr	-0.24	0.00	0.00	0.04	-863.10	0.43	-863.57
^{104}Zr	-0.24	0.00	0.00	0.02	-874.01	0.47	-873.85
^{106}Zr	-0.24	0.00	0.00	0.01	-884.18		-883.19*
^{108}Zr	-0.24	0.00	0.00	0.00	-893.16		-891.76*
^{110}Zr	0.00	0.00	0.18	-0.04	-902.46		-899.47*
^{112}Zr	0.00	0.00	0.13	-0.02	-908.79		-906.53*
^{114}Zr	-0.04	0.13	0.00	0.02	-915.50		

cluded. In Fig. 4, we show the single-particle levels of ^{110}Zr near the Fermi surface as functions of β_{32} with β_{20} fixed at zero. Due to the tetrahedral symmetry, the

TABLE III. The binding energy (relative to the ground state) for various energy minima (when they exist) in Zr isotopes obtained in the MDC-RHB calculations with the functional DD-PC1. All energies are in MeV.

Nucleus	^{100}Zr	^{102}Zr	^{104}Zr	^{106}Zr	^{108}Zr	^{110}Zr	^{112}Zr	^{114}Zr
Oblate	0.21	0.00	0.00	0.00	0.00	1.58	0.44	0.19
Pear-like			2.72	2.22	1.12	1.25	0.08	0.00
Tetrahedral			2.53	1.85	0.49	0.00	0.00	0.20
Prolate	0.00	0.10	0.63	0.89	0.53	2.55	2.02	4.02

TABLE IV. The reductions of the spherical levels (up to $j = 11/2$) to the irreducible representations of the T_d^D group. The two 2D irreducible representations of the T_d^D group are denoted by E'_1 and E'_2 , the 4D irreducible representation of the T_d^D group is denoted by G' .

j	Irreducible representations of T_d^D group
1/2	E'_1
3/2	G'
5/2	$E'_2 + G'$
7/2	$E'_1 + E'_2 + G'$
9/2	$E'_1 + 2G'$
11/2	$E'_1 + E'_2 + 2G'$

single-particle levels split into multiplets with degeneracies equal to the irreducible representations of the T_d^D group. For example, the spherical levels with $j = 1/2$ and $j = 3/2$ are two-fold and four-fold degenerate and they can be reduced to the two-dimensional (2D) irreducible representation E'_1 and four-dimensional (4D) irreducible representation G' of the T_d^D group, respectively. Such degeneracies are kept as β_{32} increases. The spherical levels with $j = 5/2$ can be reduced to the 2D irreducible representation E'_2 and 4D irreducible representation G' of the T_d^D group. These levels split into two levels with degeneracies 2 and 4, respectively, as β_{32} increases. The reduction of spherical levels (up to $j = 11/2$) to the irreducible representation of the T_d^D group are listed in Table IV. For protons, as shown in Fig. 4(a), the magic gap $Z \simeq 20$ is enhanced while the gap at $Z \simeq 28$ is suppressed as β_{32} increases. At $Z \simeq 40$ a large energy gap shows up with β_{32} increasing. From Fig. 4(b) we can see that large energy gaps appears at $N \simeq 40$ and 70 while the spherical magic gap around $N = 50$ is suppressed as β_{32} increases. Due to large energy gaps at $Z \simeq 40$ and $N \simeq 70$, a strong β_{32} effect is expected for ^{110}Zr and nearby nuclei.

In Fig. 5 we show the proton and neutron pairing energies of ^{110}Zr calculated with the functional DD-PC1. The changes of the pairing energy as a function of β_{20} are due to the variations of single-particle level density near the Fermi surface when β_{20} changes: lower level density near the Fermi surface usually leads to weaker pairing effects. When β_{30} and β_{32} deformations are not included, the weakest pairing effects are found around the prolate minimum (note that the three curves overlap around this

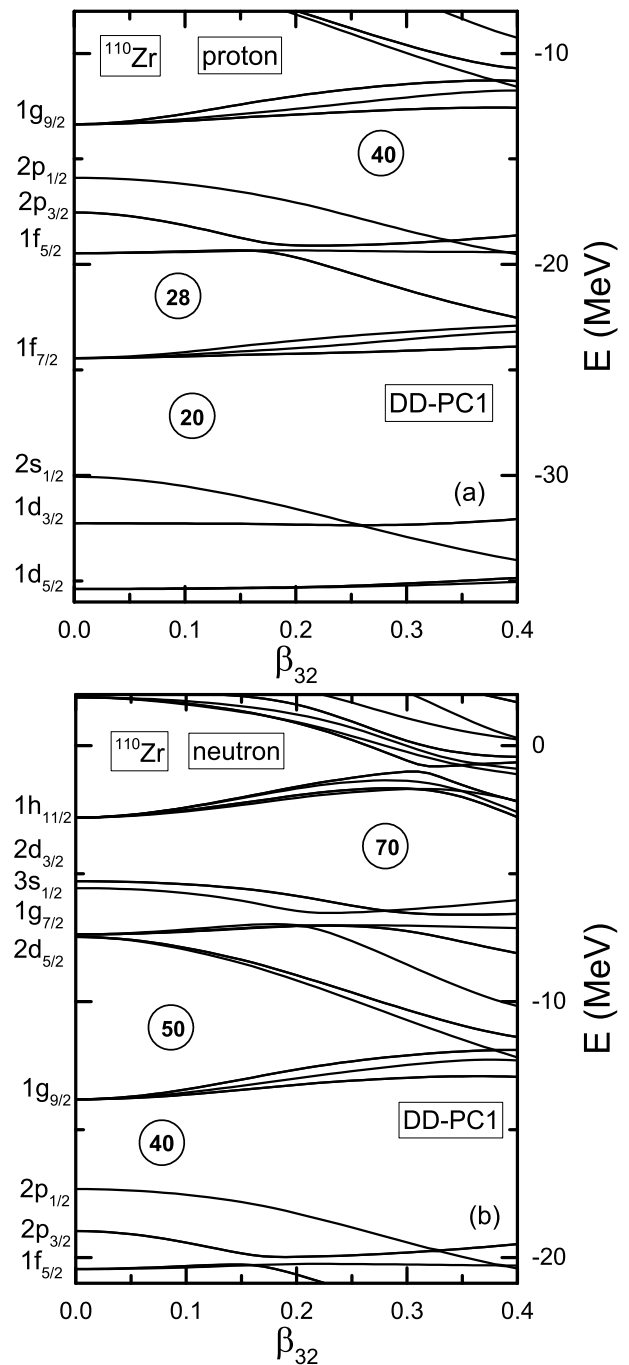


FIG. 4. The single-particle levels near the Fermi surface for protons (a) and neutrons (b) of ^{110}Zr as functions of β_{32} with β_{20} fixed at zero. The functional DD-PC1 is used in the MDC-RHB calculations.

minimum). However, the inclusion of β_{30} or β_{32} reduces the proton and neutron pairing effects around $\beta_{20} = 0$ a lot. Especially for the case of β_{32} , both proton and neutron pairing energies almost vanish around $\beta_{20} = 0$, due to the large energy gap developed at $Z \simeq 40$ and $N \simeq 70$.

From the above discussions, we know that the inclusion of β_{30} and β_{32} deformations can reduce the energies

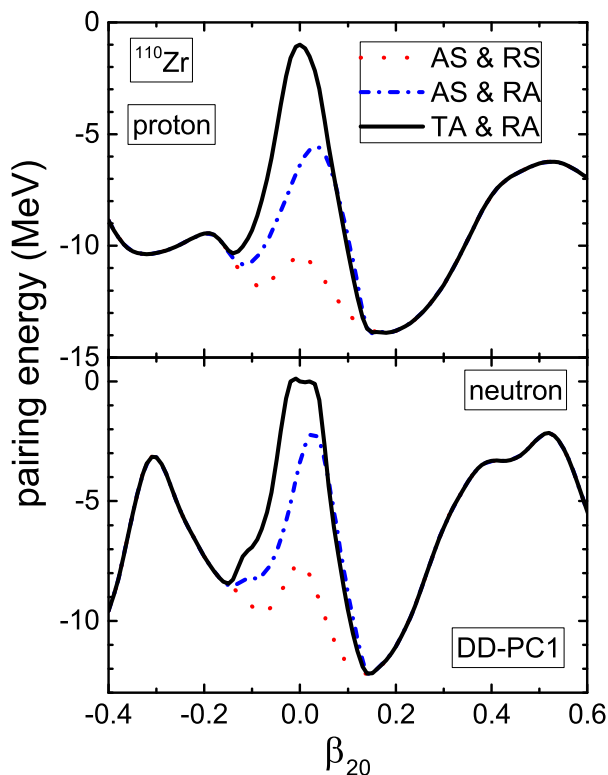


FIG. 5. (Color online) The proton and neutron pairing energies of ^{110}Zr as functions of β_{20} . The dotted line denotes the results with the axial symmetry (AS) and reflection symmetry (RS) imposed, the dash-dotted line denotes the results restricted to the AS and reflection asymmetry (RA), while the solid line represents the results with both triaxial (TA) and RA shapes allowed. The functional DD-PC1 is used in the MDC-RHB calculations.

around $\beta_{20} = 0$ for most of the neutron-rich Zr isotopes investigated here. As a result, with the functional DD-PC1, tetrahedral ground states and pear-like isomeric states are predicted for $^{110,112}\text{Zr}$ and a pear-like ground state and a tetrahedral isomeric state are predicted for ^{114}Zr . To further investigate the properties and the relation between these two minima, we calculate the potential energy surfaces (PES) of $^{106-114}\text{Zr}$ in the (β_{30}, β_{32}) plane with β_{20} fixed at zero and show them in Fig. 6. It is clearly seen that the pockets around tetrahedral minima are deeper than those around pear-like minima for $^{106-112}\text{Zr}$. For example, the minimum with $\beta_{30} \approx 0.15$ of ^{110}Zr is 1.25 MeV higher than the tetrahedral minimum with $\beta_{32} \approx 0.15$. From Fig. 6, one finds that the barriers separating the pear-like and the tetrahedral minima are very low. For ^{106}Zr , the barrier is almost invisible. For ^{108}Zr and ^{112}Zr , the barrier heights are less than 0.2 MeV. For ^{110}Zr , the barrier is higher, but still less than 0.3 MeV. In this sense, the pear-like isomeric states are rather unstable and may hardly be observed for the nuclei discussed here.

We also performed similar calculations with the func-

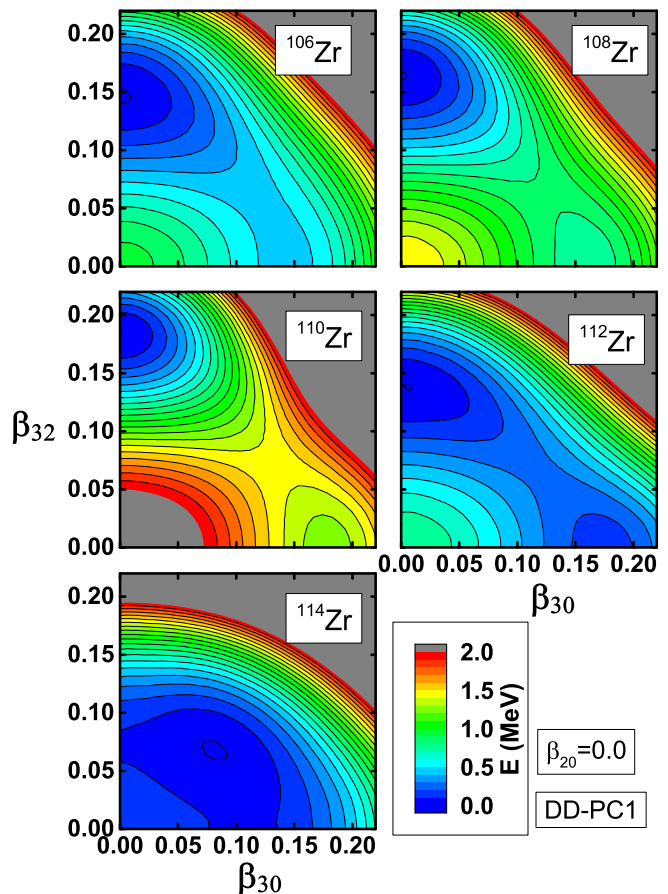


FIG. 6. (Color online) The potential energy surfaces of $^{106-114}\text{Zr}$ in the (β_{30}, β_{32}) plane with β_{20} fixed at zero. The contour interval is 0.1 MeV. The functional DD-PC1 is used in the MDC-RHB calculations.

tional PC-PK1. By examining the obtained 1D potential energy curves and 2D potential energy surfaces, it is found that with this functional and the same pairing strength as used in calculations with the functional DD-PC1 (i.e., $G_n = G_0$, $G_p = 1.12G_0$ with $G_0 = 728 \text{ MeV}\cdot\text{fm}^3$), the tetrahedral and octupole deformations have less influence on Zr isotopes than they do with DD-PC1. In this sense, the tetrahedral and octupole deformation effects are functional dependent. With these two shape degrees of freedom considered, the potential energy surfaces become softer around the local minima with $\beta_{20} \approx 0$. The most pronounced effects from the tetrahedral or octupole distortions happen in ^{110}Zr for which a spherical shape is already obtained under the assumption of axial and reflection symmetries. In the AS & RA calculations, the ground state minimum for ^{110}Zr is lowered by about 0.1 MeV and in the TA & RA calculations, the minimum corresponding to the tetrahedral shape is lower by about 0.1 MeV than that corresponds to an octupole shape.

Experimentally, low-lying spectra for even- A Zr isotopes have been established, from which it has been con-

cluded that $^{100,102,104,106,108}\text{Zr}$ are well deformed. However, there has been no such experimental information for ^{110}Zr . In some theoretical investigations (see, e.g., Ref. [138]) it is predicted that ^{110}Zr is also well deformed. In our calculations, ^{110}Zr is predicted to be tetrahedral because of the strong effects of shell closures around $Z \simeq 40$ and $N \simeq 70$.

IV. SUMMARY

We have developed a multidimensionally constrained relativistic Hartree-Bogoliubov (MDC-RHB) model in which the pairing correlations are taken into account with the Bogoliubov transformation. In this model, the nuclear shape is assumed to be invariant under the reversal of x and y axes, thus, all shape degrees of freedom $\beta_{\lambda\mu}$ with even μ are included self-consistently. A separable pairing force of finite range is adopted in this model. We solve the RHB equation in an axially deformed harmonic oscillator (ADHO) basis. The convergence of the calculated results against the basis truncation is studied and it is shown that a reasonably large ADHO basis is able to provide a desired accuracy.

We have calculated the potential energy curves ($E \sim \beta_{20}$) of neutron-rich even-even Zr isotopes with the MDC-RHB model. It is found that the β_{32} deformation plays a very important role in the isomeric or ground states of these nuclei, especially for nuclei around $N = 70$. The ground state shape of ^{110}Zr is predicted to be tetrahedral with both functionals DD-PC1 and PC-PK1. ^{112}Zr is also predicted to have a tetrahedral ground state with the functional DD-PC1. We investigated the evolution of single-particle levels in ^{110}Zr as a function of the β_{32} deformation. It is found that there are large energy gaps at $Z \simeq 40$ and $N \simeq 70$ which are responsible for the strong β_{32} distortion effect. The inclusion of β_{30} deformation can also reduce the energy around $\beta_{20} = 0$ and lead to minima with pear-like shapes for nuclei around ^{110}Zr , but these minima are rather shallow. By examining two-dimensional potential energy surfaces in the (β_{30}, β_{32}) plane with β_{20} fixed at zero, we found that the barrier separating the two minima with nonzero β_{32} or nonzero β_{30} is quite low.

ACKNOWLEDGMENTS

This work has been supported by the National Key Basic Research Program of China (Grant No. 2013CB834400), the National Natural Science Foundation of China (Grants No. 11120101005, No. 11275248, No. 11475115, No. 11525524, and No. 11621131001), and the Knowledge Innovation Project of the Chinese Academy of Sciences (Grant No. KJCX2-EW-N01). The computational results presented in this work have been obtained on the High-performance Computing Cluster of SKLTP/ITP-CAS and the ScGrid of the Supercomput-

ing Center, Computer Network Information Center of the Chinese Academy of Sciences.

Appendix A: Calculation of the pairing fields

The separable pairing force of finite range in the coordinate space reads

$$V(\mathbf{r}_1\sigma_1, \mathbf{r}_2\sigma_2, \mathbf{r}'_1\sigma'_1, \mathbf{r}'_2\sigma'_2) = -G\delta(\mathbf{R} - \mathbf{R}')P(r)P(r') \times \frac{1}{2}(1 - P_\sigma), \quad (\text{A1})$$

where $\mathbf{R} = (\mathbf{r}_1 + \mathbf{r}_2)/2$ and $\mathbf{r} = \mathbf{r}_1 - \mathbf{r}_2$ are the center-of-mass and relative coordinates, respectively. The corresponding matrix element in the axially deformed harmonic oscillator (ADHO) basis is

$$V_{12,1'2'} = \sum_{\sigma_1\sigma_2} \sum_{\sigma'_1\sigma'_2} \int d^3\mathbf{r}_1 d^3\mathbf{r}_2 d^3\mathbf{r}'_1 d^3\mathbf{r}'_2 \Phi_1^*(\mathbf{r}_1\sigma_1) \Phi_2^*(\mathbf{r}_2\sigma_2) \times V(\mathbf{r}_1\sigma_1, \mathbf{r}_2\sigma_2, \mathbf{r}'_1\sigma'_1, \mathbf{r}'_2\sigma'_2) \Phi_{1'}(\mathbf{r}'_1\sigma'_1) \Phi_{2'}(\mathbf{r}'_2\sigma'_2). \quad (\text{A2})$$

Referring to the structure of the basis wave functions Eq. (24), $V_{12,1'2'}$ can be written as a product of integrals and sums,

$$V_{12,1'2'} = (C_1 C_2)^* (C'_1 C'_2) V_{12,1'2'}^\sigma V_{12,1'2'}^z V_{12,1'2'}^\rho, \quad (\text{A3})$$

with

$$V_{12,1'2'}^\sigma = \sum_{\substack{\sigma_1\sigma_2 \\ \sigma'_1\sigma'_2}} \chi_{s_1}(\sigma_1) \chi_{s_2}(\sigma_2) \frac{1}{2}(1 - P_\sigma) \chi_{s'_1}(\sigma'_1) \chi_{s'_2}(\sigma'_2) = \frac{1}{2}(2s_1 \delta_{\sigma_1, \bar{\sigma}_2})(2s'_1 \delta_{\sigma'_1, \bar{\sigma}'_2}), \quad (\text{A4})$$

$$V_{12,1'2'}^z = \int dz_1 dz_2 dz'_1 dz'_2 \phi_{n_{z_1}}(z_1) \phi_{n_{z_2}}(z_2) \times [\delta(Z - Z') P_z(z) P_z(z')] \phi_{n'_{z_1}}(z'_1) \phi_{n'_{z_2}}(z'_2) = \sqrt{2} \sum_{N_z} \left(\sum_n M_{N_z n}^{n_{z_1} n_{z_2}} A_n \right) \left(\sum_n M_{N_z n}^{n'_{z_1} n'_{z_2}} A_n \right), \quad (\text{A5})$$

$$V_{12,1'2'}^\rho = \int d^2\rho_1 d^2\rho_2 d^2\rho'_1 d^2\rho'_2 \times R_{n_{\rho_1}}^{m_{\rho_1}}(\rho_1) R_{n_{\rho_2}}^{m_{\rho_2}}(\rho_2) \frac{1}{2\pi} e^{-i(m_{\rho_1}\varphi_1 + m_{\rho_2}\varphi_2)} \times [\delta(\boldsymbol{\rho} - \boldsymbol{\rho}') P_\rho(\rho) P_\rho(\rho')] \times R_{n'_{\rho_1}}^{m'_{\rho_1}}(\rho_1) R_{n'_{\rho_2}}^{m'_{\rho_2}}(\rho_2) \frac{1}{2\pi} e^{i(m'_{\rho_1}\varphi_1 + m'_{\rho_2}\varphi_2)} = \sqrt{2} \sum_{N_\rho M_\rho} \left(\sum_n M_{N_\rho M_\rho n}^{n_{\rho_1} m_{\rho_1} n_{\rho_2} m_{\rho_2}} B_n \right) \times \left(\sum_n M_{N_\rho M_\rho n}^{n'_{\rho_1} m'_{\rho_1} n'_{\rho_2} m'_{\rho_2}} B_n \right), \quad (\text{A6})$$

where

$$\begin{aligned} A_n &= \int_{-\infty}^{\infty} \phi_n(z) P_z(\sqrt{2}z) dz, \\ B_n &= \sqrt{2\pi} \int_0^{\infty} P_\rho(\sqrt{2}\rho) R_n^0(\rho) \rho d\rho, \end{aligned} \quad (\text{A7})$$

are constants. All these terms are in separable forms; so is the matrix element

$$V_{12,1'2'} = \sum_{N_z N_\rho M_\rho} \left(W_{12}^{N_z N_\rho M_\rho} \right)^* W_{1'2'}^{N_z N_\rho M_\rho}, \quad (\text{A8})$$

where

$$\begin{aligned} W_{12}^{N_z N_\rho M_\rho} &= (C_1 C_2) (2s_1 \delta_{\sigma_1, \bar{\sigma}_2}) \left(\sum_n M_{N_z n}^{n_{z_1} n_{z_2}} A_n \right) \\ &\times \left(\sum_n M_{N_\rho M_\rho n_0}^{n_{\rho_1} m_{l_1} n_{\rho_2} m_{l_2}} B_n \right). \end{aligned} \quad (\text{A9})$$

The Talmi-Moshinski brackets are given in the next appendix.

Appendix B: The Talmi-Moshinski brackets

As usual the Talmi-Moshinski brackets are calculated by the generating function method. Here we only show the final results and the details can be found in Ref. [169].

The one-dimensional Talmi-Moshinski bracket reads

$$\begin{aligned} M_{N_z n_z}^{n_{z_1} n_{z_2}} &= \int_{-\infty}^{\infty} dz_1 dz_2 \phi_{n_{z_1}}(z_1) \phi_{n_{z_2}}(z_2) \phi_{N_z}(z_+) \phi_{n_z}(z_-) \\ &= \frac{1}{\sqrt{2^{N_z+n_z}}} \sqrt{\frac{n_{z_1}! n_{z_2}!}{N_z! n_z!}} \delta_{n_{z_1}+n_{z_2}, N_z+n_z} \\ &\times \sum_{s=0}^{n_z} (-1)^s \binom{N_z}{n_{z_1} - n_z + s} \binom{n_z}{s}, \end{aligned} \quad (\text{B1})$$

where $z_+ = \frac{1}{\sqrt{2}}(z_1 + z_2)$ and $z_- = \frac{1}{\sqrt{2}}(z_1 - z_2)$.

The two-dimensional Talmi-Moshinski bracket is

$$\begin{aligned} M_{N M n m}^{n_1 m_1 n_2 m_2} &= \int_0^{\infty} \rho_1 d\rho_1 \int_0^{2\pi} d\varphi_1 \int_0^{\infty} \rho_2 d\rho_2 \int_0^{2\pi} d\varphi_2 R_{n_1}^{m_1}(\rho_1) e^{-im_1\varphi_1} R_{n_2}^{m_2}(\rho_2) e^{-im_2\varphi_2} R_N^M(\rho_+) e^{iM\varphi_+} R_n^m(\rho_-) e^{im\varphi_-} \\ &= \delta_{M+m, m_1+m_2} \delta_{2n_1+|m_1|+2n_2+|m_2|, 2N+|M|+2n+|m|} \frac{(-1)^{n_1+n_2+N+n}}{\sqrt{2^{2n_1+|m_1|+2n_2+|m_2|}}} \sqrt{\frac{N!(N+|M|)!n!(n+|m|)!}{n_1!(n_1+|m_1|)!n_2!(n_2+|m_2|)!}} \\ &\times \sum_{\substack{p_1, q_1, r_1, s_1 \\ p_2, q_2, r_2, s_2}}^{n_1 n_2} \sum_{t_1 t_2}^{|m_1| |m_2|} (-1)^{r_2+s_2+|m_2|-t_2} \delta_{p_1 r_1 s_1 t_1} \binom{|m_1|}{t_1} \binom{|m_2|}{t_2} \binom{n_1}{p_1 \ q_1 \ r_1 \ s_1} \binom{n_2}{p_2 \ q_2 \ r_2 \ s_2}, \end{aligned} \quad (\text{B2})$$

where the variables $(\rho_{\pm}, \varphi_{\pm})$ are defined as

$$\begin{aligned} \rho_{\pm} \cos \varphi_{\pm} &= \frac{1}{\sqrt{2}} (\rho_1 \cos \varphi_1 \pm \rho_2 \cos \varphi_2), \\ \rho_{\pm} \sin \varphi_{\pm} &= \frac{1}{\sqrt{2}} (\rho_1 \sin \varphi_1 \pm \rho_2 \sin \varphi_2). \end{aligned} \quad (\text{B3})$$

The multinomial coefficients are

$$\binom{q}{p_1 \ p_2 \ p_3 \ \dots \ p_n} = \delta_{\sum_k p_k, q} \frac{q!}{\prod_{k=1}^n p_k}, \quad (\text{B4})$$

and the Kronecker δ 's are

$$\delta_{p_2 r_2 s_2 t_2}^{p_1 r_1 s_1 t_1} = \begin{cases} \delta_{t_1+t_2, N-(p_1+s_1)-(p_2+s_2)+(|M|+M)/2} \delta_{0, N-(p_1+r_1)-(p_2+r_2)+\frac{1}{2}(|M|-M)}, & m_1 m_2 \geq 0, \\ \delta_{t_1, N-(p_1+s_1)-(p_2+s_2)+(|M|+M)/2} \delta_{t_2, N-(p_1+r_1)-(p_2+r_2)+(|M|-M)/2}, & m_1 m_2 \leq 0. \end{cases} \quad (\text{B5})$$

[1] A. Bohr and B. R. Mottelson, *Nuclear Structure*, 1st ed., Vol. I (Benjamin, New York, 1969).

[2] A. Bohr and B. R. Mottelson, *Nuclear Structure*, 1st

- ed., Vol. II (Benjamin, New York, 1975).
- [3] S. Frauendorf and J. Meng, *Nucl. Phys. A* **617**, 131 (1997).
- [4] S. W. Odegard, G. B. Hagemann, D. R. Jensen, M. Bergstroem, B. Herskind, G. Sletten, S. Toermænen, J. N. Wilson, P. O. Tjom, I. Hamamoto, K. Spohr, H. Huebel, A. Goergen, G. Schoenwasser, A. Bracco, S. Leoni, A. Maj, C. M. Petrache, P. Bednarczyk, and D. Curien, *Phys. Rev. Lett.* **86**, 5866 (2001).
- [5] K. Starosta, T. Koike, C. J. Chiara, D. B. Fossan, D. R. LaFosse, A. A. Hecht, C. W. Beausang, M. A. Caprio, J. R. Cooper, R. Krucken, J. R. Novak, N. V. Zamfir, K. E. Zyromski, D. J. Hartley, D. L. Balabanski, J.-y. Zhang, S. Frauendorf, and V. I. Dimitrov, *Phys. Rev. Lett.* **86**, 971 (2001).
- [6] J. Meng, J. Peng, S. Q. Zhang, and S.-G. Zhou, *Phys. Rev. C* **73**, 037303 (2006).
- [7] A. D. Ayangeakaa, U. Garg, M. D. Anthony, S. Frauendorf, J. T. Matta, B. K. Nayak, D. Patel, Q. B. Chen, S. Q. Zhang, P. W. Zhao, B. Qi, J. Meng, R. V. F. Janssens, M. P. Carpenter, C. J. Chiara, F. G. Kondev, T. Lauritsen, D. Seweryniak, S. Zhu, S. S. Ghugre, and R. Palit, *Phys. Rev. Lett.* **110**, 172504 (2013).
- [8] E. O. Lieder, R. M. Lieder, R. A. Bark, Q. B. Chen, S. Q. Zhang, J. Meng, E. A. Lawrie, J. J. Lawrie, S. P. Bvumbi, N. Y. Kheswa, S. S. Ntshangase, T. E. Madiba, P. L. Masiteng, S. M. Mullins, S. Murray, P. Papka, D. G. Roux, O. Shirinda, Z. H. Zhang, P. W. Zhao, Z. P. Li, J. Peng, B. Qi, S. Y. Wang, Z. G. Xiao, and C. Xu, *Phys. Rev. Lett.* **112**, 202502 (2014).
- [9] I. Kuti, Q. B. Chen, J. Timar, D. Sohler, S. Q. Zhang, Z. H. Zhang, P. W. Zhao, J. Meng, K. Starosta, T. Koike, E. S. Paul, D. B. Fossan, and C. Vaman, *Phys. Rev. Lett.* **113**, 032501 (2014).
- [10] D. Tonev, M. S. Yavahchova, N. Goutev, G. de Angelis, P. Petkov, R. K. Bhowmik, R. P. Singh, S. Muralithar, N. Madhavan, R. Kumar, M. Kumar Raju, J. Kaur, G. Mohanto, A. Singh, N. Kaur, R. Garg, A. Shukla, T. K. Marinov, and S. Brant, *Phys. Rev. Lett.* **112**, 052501 (2014).
- [11] C. Liu, S. Y. Wang, R. A. Bark, S. Q. Zhang, J. Meng, B. Qi, P. Jones, S. M. Wyngaardt, J. Zhao, C. Xu, S.-G. Zhou, S. Wang, D. P. Sun, L. Liu, Z. Q. Li, N. B. Zhang, H. Jia, X. Q. Li, H. Hua, Q. B. Chen, Z. G. Xiao, H. J. Li, L. H. Zhu, T. D. Bucher, T. Dinoko, J. Easton, K. Juhász, A. Kamblawe, E. Khaleel, N. Khumalo, E. A. Lawrie, J. J. Lawrie, S. N. T. Majola, S. M. Mullins, S. Murray, J. Ndayishimye, D. Negi, S. P. Noncolela, S. S. Ntshangase, B. M. Nyakó, J. N. Orce, P. Papka, J. F. Sharpey-Schafer, O. Shirinda, P. Sithole, M. A. Stankiewicz, and M. Wiedeking, *Phys. Rev. Lett.* **116**, 112501 (2016).
- [12] R. Bengtsson, H. Frisk, F. R. May, and J. A. Pinston, *Nucl. Phys. A* **415**, 189 (1984).
- [13] Y. Liu, Y. Ma, H. Yang, and S. Zhou, *Phys. Rev. C* **52**, 2514 (1995).
- [14] Y. Liu, J. Lu, Y. Ma, S. Zhou, and H. Zheng, *Phys. Rev. C* **54**, 719 (1996).
- [15] S. G. Zhou, Y. Z. Liu, Y. J. Ma, and C. X. Yang, *J. Phys. G: Nucl. Phys.* **22**, 415 (1996).
- [16] L. L. Riedinger, H. Q. Jin, W. Reviol, J.-Y. Zhang, R. A. Bark, G. B. Hagemann, and P. B. Semmes, *Prog. Part. Nucl. Phys.* **38**, 251 (1997).
- [17] Y. Liu, J. Lu, Y. Ma, G. Zhao, H. Zheng, and S. Zhou, *Phys. Rev. C* **58**, 1849 (1998).
- [18] A. V. Afanasjev, D. B. Fossan, G. J. Lane, and I. Ragnarsson, *Phys. Rep.* **322**, 1 (1999).
- [19] P. A. Butler and W. Nazarewicz, *Rev. Mod. Phys.* **68**, 349 (1996).
- [20] P. Möller, R. Bengtsson, B. G. Carlsson, P. Olivius, T. Ichikawa, H. Sagawa, and A. Iwamoto, *At. Data Nucl. Data Tables* **94**, 758 (2008).
- [21] S. E. Agbemava, A. V. Afanasjev, and P. Ring, *Phys. Rev. C* **93**, 044304 (2016).
- [22] T. M. Shneidman, G. G. Adamian, N. V. Antonenko, R. V. Jolos, and W. Scheid, *Phys. Rev. C* **67**, 014313 (2003).
- [23] T. M. Shneidman, G. G. Adamian, N. V. Antonenko, and R. V. Jolos, *Phys. Rev. C* **74**, 034316 (2006).
- [24] S. Wang, H. Hua, J. Meng, Z. H. Li, S. Q. Zhang, F. R. Xu, H. L. Liu, Y. L. Ye, D. X. Jiang, T. Zheng, Q. J. Wang, Z. Q. Chen, C. E. Wu, G. L. Zhang, D. Y. Pang, J. Wang, J. L. Lou, B. Guo, G. Jin, S. G. Zhou, L. H. Zhu, X. G. Wu, G. S. Li, S. X. Wen, C. Y. He, X. Z. Cui, and Y. Liu, *Phys. Rev. C* **72**, 024317 (2005).
- [25] D. Yang, J.-B. Lu, Y.-Z. Liu, L.-L. Wang, K.-Y. Ma, C.-D. Yang, D.-K. Han, Y.-X. Zhao, Y.-J. Ma, L.-H. Zhu, X.-G. Wu, and G.-S. Li, *Chin. Phys. Lett.* **26**, 082101 (2009).
- [26] L. M. Robledo and G. F. Bertsch, *Phys. Rev. C* **84**, 054302 (2011).
- [27] S. J. Zhu, M. Sakhaee, J. H. Hamilton, A. V. Ramayya, N. T. Brewer, J. K. Hwang, S. H. Liu, E. Y. Yeoh, Z. G. Xiao, Q. Xu, Z. Zhang, Y. X. Luo, J. O. Rasmussen, I. Y. Lee, K. Li, and W. C. Ma, *Phys. Rev. C* **85**, 014330 (2012).
- [28] S. J. Zhu, J. H. Hamilton, A. V. Ramayya, J. K. Hwang, Y. J. Chen, L. Y. Zhu, H. J. Li, Z. G. Xiao, E. Y. Yeoh, J. G. Wang, Y. X. Luo, S. H. Liu, J. O. Rasmussen, and I. Y. Lee, in *Nuclear Structure in China 2012: Proceedings of the 14th National Conference on Nuclear Structure in China (NSC2012)*, edited by J. Meng, C.-W. Shen, E.-G. Zhao, and S.-G. Zhou (World Scientific, Singapore, 2012) pp. 348–356.
- [29] K. Nomura, D. Vretenar, and B.-N. Lu, *Phys. Rev. C* **88**, 021303(R) (2013).
- [30] K. Nomura, D. Vretenar, T. Nikšić, and B.-N. Lu, *Phys. Rev. C* **89**, 024312 (2014).
- [31] K. Nomura, R. Rodriguez-Guzman, and L. M. Robledo, *Phys. Rev. C* **92**, 014312 (2015).
- [32] L. P. Gaffney, P. A. Butler, M. Scheck, A. B. Hayes, F. Wenander, M. Albers, B. Bastin, C. Bauer, A. Blazhev, S. Bonig, N. Bree, J. Cederkall, T. Chupp, D. Cline, T. E. Cocolios, T. Davinson, H. De Witte, J. Diriken, T. Grahn, A. Herzan, M. Huyse, D. G. Jenkins, D. T. Joss, N. Kesteloot, J. Konki, M. Kowalczyk, T. Kroll, E. Kwan, R. Lutter, K. Moschner, P. Napiorkowski, J. Pakarinen, M. Pfeiffer, D. Radeck, P. Reiter, K. Reynders, S. V. Rigby, L. M. Robledo, M. Rudigier, S. Sambi, M. Seidlitz, B. Siebeck, T. Stora, P. Thoele, P. Van Duppen, M. J. Vermeulen, M. von Schmid, D. Voulot, N. Warr, K. Wimmer, K. Wrzosek-Lipska, C. Y. Wu, and M. Zielinska, *Nature* **497**, 199 (2013).
- [33] B. Bucher, S. Zhu, C. Y. Wu, R. V. F. Janssens, D. Cline, A. B. Hayes, M. Albers, A. D. Ayangeakaa, P. A. Butler, C. M. Campbell, M. P. Carpenter, C. J. Chiara, J. A. Clark, H. L. Crawford, M. Cromaz, H. M.

- David, C. Dickerson, E. T. Gregor, J. Harker, C. R. Hoffman, B. P. Kay, F. G. Kondev, A. Korichi, T. Lauritsen, A. O. Macchiavelli, R. C. Pardo, A. Richard, M. A. Riley, G. Savard, M. Scheck, D. Seweryniak, M. K. Smith, R. Vondrasek, and A. Wiens, *Phys. Rev. Lett.* **116**, 112503 (2016).
- [34] B.-N. Lu, E.-G. Zhao, and S.-G. Zhou, *Phys. Rev. C* **85**, 011301(R) (2012).
- [35] I. Hamamoto, B. Mottelson, H. Xie, and X. Z. Zhang, *Z. Phys. D* **21**, 163 (1991).
- [36] J. Skalski, *Phys. Rev. C* **43**, 140 (1991).
- [37] X. Li and J. Dudek, *Phys. Rev. C* **49**, R1250 (1994).
- [38] S. Takami, K. Yabana, and M. Matsuo, *Phys. Lett. B* **431**, 242 (1998).
- [39] M. Yamagami, K. Matsuyanagi, and M. Matsuo, *Nucl. Phys. A* **693**, 579 (2001).
- [40] J. Dudek, A. Gozdz, N. Schunck, and M. Miskiewicz, *Phys. Rev. Lett.* **88**, 252502 (2002).
- [41] J. Dudek, D. Curien, N. Dubray, J. Dobaczewski, V. Pangon, P. Olbratowski, and N. Schunck, *Phys. Rev. Lett.* **97**, 072501 (2006).
- [42] P. Olbratowski, J. Dobaczewski, P. Powalowski, M. Sadziak, and K. Zborecki, *Int. J. Mod. Phys. E* **15**, 333 (2006).
- [43] K. Zborecki, P. Magierski, P.-H. Heenen, and N. Schunck, *Phys. Rev. C* **74**, 051302(R) (2006).
- [44] J. Dudek, A. Gozdz, K. Mazurek, and H. Moliq, *J. Phys. G: Nucl. Phys.* **37**, 064032 (2010).
- [45] J. Dudek, J. Dobaczewski, N. Dubray, A. Gozdz, V. Pangon, and N. Schunck, *Int. J. Mod. Phys. E* **16**, 516 (2007).
- [46] J. Dudek, A. Gozdz, and N. Schunck, *Acta Phys. Pol. B* **34**, 2491 (2003).
- [47] W. D. Heiss, R. A. Lynch, and R. G. Nazmitdinov, *Phys. Rev. C* **60**, 034303 (1999).
- [48] K.-i. Arita and Y. Mukumoto, *Phys. Rev. C* **89**, 054308 (2014).
- [49] N. Schunck, J. Dudek, A. Gozdz, and P. H. Regan, *Phys. Rev. C* **69**, 061305(R) (2004).
- [50] J. Dudek, D. Curien, D. Rouvel, K. Mazurek, Y. R. Shimizu, and S. Tagami, *Phys. Scr.* **89**, 054007 (2014).
- [51] K. Zborecki, P.-H. Heenen, and P. Magierski, *Phys. Rev. C* **79**, 014319 (2009).
- [52] R. Bijker and F. Iachello, *Phys. Rev. Lett.* **112**, 152501 (2014).
- [53] Y. Chen and Z. Gao, *Nucl. Phys. Rev.* **30**, 278 (2013).
- [54] Y. S. Chen and Z.-C. Gao, *Nucl. Phys. A* **834**, 378c (2010).
- [55] Z.-C. Gao, Y.-S. Chen, and J. Meng, *Chin. Phys. Lett.* **21**, 806 (2004).
- [56] S. Tagami, Y. R. Shimizu, and J. Dudek, *Phys. Rev. C* **87**, 054306 (2013).
- [57] S. Tagami, Y. R. Shimizu, and J. Dudek, *J. Phys. G: Nucl. Part. Phys.* **42**, 015106 (2015).
- [58] R. A. Bark, J. F. Sharpey-Schafer, S. M. Maliage, T. E. Madiba, F. S. Komati, E. A. Lawrie, J. J. Lawrie, R. Lindsay, P. Mahe, S. M. Mullins, S. H. T. Murray, N. J. Ncapayi, T. M. Ramashidza, F. D. Smit, and P. Vymers, *Phys. Rev. Lett.* **104**, 022501 (2010).
- [59] M. Jentschel, W. Urban, J. Krempel, D. Tonev, J. Dudek, D. Curien, B. Lauss, G. de Angelis, and P. Petkov, *Phys. Rev. Lett.* **104**, 222502 (2010).
- [60] Q. T. Doan, A. Vancraeynest, O. Stézowski, D. Guinet, D. Curien, J. Dudek, P. Lauthesse, G. Lehaut, N. Redon, C. Schmitt, G. Duchêne, B. Gall, H. Moliq, J. Piot, P. T. Greenlees, U. Jakobsson, R. Julin, S. Juutinen, P. Jones, S. Ketelhut, M. Nyman, P. Peura, P. Rakhila, A. Gózdź, K. Mazurek, N. Schunck, K. Zuber, P. Bednarczyk, A. Maj, A. Astier, I. Deloncle, D. Verney, G. de Angelis, and J. Gerl, *Phys. Rev. C* **82**, 067306 (2010).
- [61] S. S. Ntshangase, R. A. Bark, D. G. Aschman, S. Bvumbi, P. Datta, P. M. Davidson, T. S. Dinoko, M. E. A. Elbasher, K. Juhász, E. M. A. Khaleel, A. Krasznahorkay, E. A. Lawrie, J. J. Lawrie, R. M. Lieder, S. N. T. Majola, P. L. Masiteng, H. Mohammed, S. M. Mullins, P. Nieminen, B. M. Nyakó, P. Papka, D. G. Roux, J. F. Sharpey-Schafer, O. Shirinda, M. A. Stankiewicz, J. Timár, and A. N. Wilson, *Phys. Rev. C* **82**, 041305(R) (2010).
- [62] T. Sumikama, K. Yoshinaga, H. Watanabe, S. Nishimura, Y. Miyashita, K. Yamaguchi, K. Sugimoto, J. Chiba, Z. Li, H. Baba, J. S. Berryman, N. Blasi, A. Bracco, F. Camera, P. Doornenbal, S. Go, T. Hashimoto, S. Hayakawa, C. Hinke, E. Ideguchi, T. Isobe, Y. Ito, D. G. Jenkins, Y. Kawada, N. Kobayashi, Y. Kondo, R. Krücken, S. Kubono, G. Lorusso, T. Nakano, M. Kurata-Nishimura, A. Odahara, H. J. Ong, S. Ota, Z. Podolyák, H. Sakurai, H. Scheit, K. Steiger, D. Steppenbeck, S. Takano, A. Takashima, K. Tajiri, T. Teranishi, Y. Wakabayashi, P. M. Walker, O. Wieland, and H. Yamaguchi, *Phys. Rev. Lett.* **106**, 202501 (2011).
- [63] Y.-X. Liu, Y. Sun, X.-H. Zhou, Y.-H. Zhang, S.-Y. Yu, Y.-C. Yang, and H. Jin, *Nucl. Phys. A* **858**, 11 (2011).
- [64] Y. Liu, S. Yu, and Y. Sun, *Sci. China Phys. Mech. Astron.* **58**, 112003 (2015).
- [65] A. V. Afanasjev, T. L. Khoo, S. Frauendorf, G. A. Lalazissis, and I. Ahmad, *Phys. Rev. C* **67**, 024309 (2003).
- [66] M. Leino and F. P. Hessberger, *Annu. Rev. Nucl. Part. Sci.* **54**, 175 (2004).
- [67] R.-D. Herzberg, P. T. Greenlees, P. A. Butler, G. D. Jones, M. Venhart, I. G. Darby, S. Eeckhaudt, K. Eskola, T. Grahm, C. Gray-Jones, F. P. Hessberger, P. Jones, R. Julin, S. Juutinen, S. Ketelhut, W. Korten, M. Leino, A.-P. Leppanen, S. Moon, M. Nyman, R. D. Page, J. Pakarinen, A. Pritchard, P. Rakhila, J. Saren, C. Scholey, A. Steer, Y. Sun, C. Theisen, and J. Uusitalo, *Nature* **442**, 896 (2006).
- [68] R.-D. Herzberg and P. Greenlees, *Prog. Part. Nucl. Phys.* **61**, 674 (2008).
- [69] Z.-H. Zhang, J.-Y. Zeng, E.-G. Zhao, and S.-G. Zhou, *Phys. Rev. C* **83**, 011304(R) (2011).
- [70] Z.-H. Zhang, X.-T. He, J.-Y. Zeng, E.-G. Zhao, and S.-G. Zhou, *Phys. Rev. C* **85**, 014324 (2012).
- [71] Z.-H. Zhang, J. Meng, E.-G. Zhao, and S.-G. Zhou, *Phys. Rev. C* **87**, 054308 (2013).
- [72] H. L. Liu, P. M. Walker, and F. R. Xu, *Phys. Rev. C* **89**, 044304 (2014).
- [73] Y. Shi, J. Dobaczewski, and P. T. Greenlees, *Phys. Rev. C* **89**, 034309 (2014).
- [74] H.-L. Wang, Q.-Z. Chai, J.-G. Jiang, and M.-L. Liu, *Chin. Phys. C* **38**, 074101 (2014).
- [75] A. V. Afanasjev, *Phys. Scr.* **89**, 054001 (2014).
- [76] S. E. Agbemava, A. V. Afanasjev, T. Nakatsukasa, and P. Ring, *Phys. Rev. C* **92**, 054310 (2015).
- [77] A. V. Afanasjev, *J. Phys. G: Nucl. Part. Phys.* **42**,

- 034002 (2015).
- [78] Y.-C. Li and X.-T. He, *Sci. China Phys. Mech. Astron.* **59**, 672001 (2016).
- [79] A. P. Robinson, T. L. Khoo, I. Ahmad, S. K. Tandel, F. G. Kondev, T. Nakatsukasa, D. Seweryniak, M. Asai, B. B. Back, M. P. Carpenter, P. Chowdhury, C. N. Davids, S. Eeckhaudt, J. P. Greene, P. T. Greenlees, S. Gros, A. Heinz, R.-D. Herzberg, R. V. F. Janssens, G. D. Jones, T. Lauritsen, C. J. Lister, D. Peterson, J. Qian, U. S. Tandel, X. Wang, and S. Zhu, *Phys. Rev. C* **78**, 034308 (2008).
- [80] Y.-S. Chen, Y. Sun, and Z.-C. Gao, *Phys. Rev. C* **77**, 061305(R) (2008).
- [81] J. Zhao, B.-N. Lu, E.-G. Zhao, and S.-G. Zhou, *Phys. Rev. C* **86**, 057304 (2012).
- [82] B. D. Serot and J. D. Walecka, *Adv. Nucl. Phys.* **16**, 1 (1986).
- [83] P. G. Reinhard, *Rep. Prog. Phys.* **52**, 439 (1989).
- [84] P. Ring, *Prog. Part. Nucl. Phys.* **37**, 193 (1996).
- [85] M. Bender, P.-H. Heenen, and P.-G. Reinhard, *Rev. Mod. Phys.* **75**, 121 (2003).
- [86] D. Vretenar, A. V. Afanasjev, G. A. Lalazissis, and P. Ring, *Phys. Rep.* **409**, 101 (2005).
- [87] J. Meng, H. Toki, S. G. Zhou, S. Q. Zhang, W. H. Long, and L. S. Geng, *Prog. Part. Nucl. Phys.* **57**, 470 (2006).
- [88] N. Paar, D. Vretenar, and G. Colo, *Rep. Prog. Phys.* **70**, 691 (2007).
- [89] T. Nikšić, D. Vretenar, and P. Ring, *Prog. Part. Nucl. Phys.* **66**, 519 (2011).
- [90] H. Liang, J. Meng, and S.-G. Zhou, *Phys. Rep.* **570**, 1 (2015).
- [91] J. Meng and S. G. Zhou, *J. Phys. G: Nucl. Part. Phys.* **42**, 093101 (2015).
- [92] J. Meng, ed., *Relativistic Density Functional for Nuclear Structure*, International Review of Nuclear Physics, Vol. 10 (World Scientific, 2016).
- [93] A. V. Afanasjev, S. E. Agbemava, D. Ray, and P. Ring, *Phys. Lett. B* **726**, 680 (2013).
- [94] S. E. Agbemava, A. V. Afanasjev, D. Ray, and P. Ring, *Phys. Rev. C* **89**, 054320 (2014).
- [95] K. Q. Lu, Z. X. Li, Z. P. Li, J. M. Yao, and J. Meng, *Phys. Rev. C* **91**, 027304 (2015).
- [96] A. V. Afanasjev and S. E. Agbemava, *Phys. Rev. C* **93**, 054310 (2016).
- [97] B.-N. Lu, J. Zhao, E.-G. Zhao, and S.-G. Zhou, *J. Phys.: Conf. Ser.* **492**, 012014 (2014).
- [98] B.-N. Lu, J. Zhao, E.-G. Zhao, and S.-G. Zhou, *Phys. Rev. C* **89**, 014323 (2014).
- [99] B.-N. Lu, J. Zhao, E.-G. Zhao, and S.-G. Zhou, *Phys. Scr.* **89**, 054028 (2014).
- [100] B.-N. Lu, J. Zhao, E.-G. Zhao, and S.-G. Zhou, *EPJ Web Conf.* **38**, 05003 (2012).
- [101] J. Zhao, B.-N. Lu, D. Vretenar, E.-G. Zhao, and S.-G. Zhou, *Phys. Rev. C* **91**, 014321 (2015).
- [102] J. Zhao, B.-N. Lu, T. Nikšić, D. Vretenar, and S.-G. Zhou, *Phys. Rev. C* **93**, 044315 (2016).
- [103] B.-N. Lu, E.-G. Zhao, and S.-G. Zhou, *Phys. Rev. C* **84**, 014328 (2011).
- [104] B.-N. Lu, E. Hiyama, H. Sagawa, and S.-G. Zhou, *Phys. Rev. C* **89**, 044307 (2014).
- [105] L.-L. Li, B.-N. Lu, N. Wang, K. Wen, C.-J. Xia, Z.-H. Zhang, J. Zhao, E.-G. Zhao, and S.-G. Zhou, *Nucl. Phys. Rev.* **31**, 253 (2014), (in Chinese).
- [106] B.-N. Lu, J. Zhao, E.-G. Zhao, and S.-G. Zhou, in *Relativistic Density Functional for Nuclear Structure*, International Review of Nuclear Physics, Vol. 10, edited by J. Meng (World Scientific, 2016) Chap. 5. Superheavy nuclei and fission barriers, pp. 171–217.
- [107] S.-G. Zhou, *Phys. Scr.* **91**, 063008 (2016).
- [108] Y. Tian and Z.-Y. Ma, *Chin. Phys. Lett.* **23**, 3226 (2006).
- [109] Y. Tian, Z. Y. Ma, and P. Ring, *Phys. Lett. B* **676**, 44 (2009).
- [110] Y. Tian, Z.-y. Ma, and P. Ring, *Phys. Rev. C* **80**, 024313 (2009).
- [111] T. Nikšić, D. Vretenar, and P. Ring, *Phys. Rev. C* **78**, 034318 (2008).
- [112] J. Zhao, B.-N. Lu, T. Nikšić, and D. Vretenar, *Phys. Rev. C* **92**, 064315 (2015).
- [113] B. A. Nikolaus, T. Hoch, and D. G. Madland, *Phys. Rev. C* **46**, 1757 (1992).
- [114] T. Burvenich, D. G. Madland, J. A. Maruhn, and P.-G. Reinhard, *Phys. Rev. C* **65**, 044308 (2002).
- [115] J. Boguta and A. R. Bodmer, *Nucl. Phys. A* **292**, 413 (1977).
- [116] R. Brockmann and H. Toki, *Phys. Rev. Lett.* **68**, 3408 (1992).
- [117] Y. Sugahara and H. Toki, *Nucl. Phys. A* **579**, 557 (1994).
- [118] C. Fuchs, H. Lenske, and H. H. Wolter, *Phys. Rev. C* **52**, 3043 (1995).
- [119] T. Nikšić, D. Vretenar, P. Finelli, and P. Ring, *Phys. Rev. C* **66**, 024306 (2002).
- [120] H. Kucharek and P. Ring, *Z. Phys. A* **339**, 23 (1991).
- [121] M. Serra and P. Ring, *Phys. Rev. C* **65**, 064324 (2002).
- [122] Y. K. Gambhir, P. Ring, and A. Thimet, *Ann. Phys. (NY)* **198**, 132 (1990).
- [123] M. Warda, J. L. Egido, L. M. Robledo, and K. Pomorski, *Phys. Rev. C* **66**, 014310 (2002).
- [124] J. Skalski, S. Mizutori, and W. Nazarewicz, *Nucl. Phys. A* **617**, 282 (1997).
- [125] G. Lalazissis, S. Raman, and P. Ring, *At. Data Nucl. Data Tables* **71**, 1 (1999).
- [126] F. R. Xu, P. M. Walker, and R. Wyss, *Phys. Rev. C* **65**, 021303(R) (2002).
- [127] L. Geng, H. Toki, S. Sugimoto, and J. Meng, *Prog. Theo. Phys.* **110**, 921 (2003).
- [128] S. Verma, P. A. Dar, and R. Devi, *Phys. Rev. C* **77**, 024308 (2008).
- [129] M. Bender, K. Bennaceur, T. Duguet, P. H. Heenen, T. Lesinski, and J. Meyer, *Phys. Rev. C* **80**, 064302 (2009).
- [130] R. Rodríguez-Guzmán, P. Sarriguren, L. M. Robledo, and S. Perez-Martin, *Phys. Lett. B* **691**, 202 (2010).
- [131] G.-X. Dong, S.-Y. Yu, Y.-X. Liu, C.-W. Shen, and Y.-S. Dong, *Sci. China Phys. Mech. Astron.* **53**, 106 (2010).
- [132] G.-X. Dong, S.-Y. Yu, Y.-X. Liu, and C.-W. Shen, *Commun. Theor. Phys.* **56**, 922 (2011).
- [133] P. Mali, *Int. J. Mod. Phys. E* **20**, 2293 (2011).
- [134] Y. Shi, P. M. Walker, and F. R. Xu, *Phys. Rev. C* **85**, 027307 (2012).
- [135] J. Xiang, Z. Li, Z. Li, J. Yao, and J. Meng, *Nucl. Phys. A* **873**, 1 (2012).
- [136] H. Mei, J. Xiang, J. M. Yao, Z. P. Li, and J. Meng, *Phys. Rev. C* **85**, 034321 (2012).
- [137] Y.-X. Liu and Y. Sun, *J. Phys.: Conf. Ser.* **420**, 012046 (2013).
- [138] T. Togashi, Y. Tsunoda, T. Otsuka, and N. Shimizu,

- Phys. Rev. Lett.* **117**, 172502 (2016).
- [139] J. Xiang, J. M. Yao, Y. Fu, Z. H. Wang, Z. P. Li, and W. H. Long, *Phys. Rev. C* **93**, 054324 (2016).
- [140] C. Kremer, S. Aslanidou, S. Bassauer, M. Hilcker, A. Krugmann, P. von Neumann-Cosel, T. Otsuka, N. Pietralla, V. Y. Ponomarev, N. Shimizu, M. Singer, G. Steinhilber, T. Togashi, Y. Tsunoda, V. Werner, and M. Zweidinger, *Phys. Rev. Lett.* **117**, 172503 (2016).
- [141] K. Nomura, R. Rodríguez-Guzmán, and L. M. Robledo, *Phys. Rev. C* **94**, 044314 (2016).
- [142] K.-L. Kratz, J.-P. Bitouzet, F.-K. Thielemann, P. Möller, and B. Pfeiffer, *ApJ* **403**, 216 (1993).
- [143] J. Dobaczewski, I. Hamamoto, W. Nazarewicz, and J. A. Sheikh, *Phys. Rev. Lett.* **72**, 981 (1994).
- [144] B. Chen, J. Dobaczewski, K.-L. Kratz, K. Langanke, B. Pfeiffer, F.-K. Thielemann, and P. Vogel, *Phys. Lett. B* **355**, 37 (1995).
- [145] J. M. Pearson, R. C. Nayak, and S. Goriely, *Phys. Lett. B* **387**, 455 (1996).
- [146] J. Dobaczewski, W. Nazarewicz, T. R. Werner, J. F. Berger, C. R. Chinn, and J. Dechargé, *Phys. Rev. C* **53**, 2809 (1996).
- [147] B. Pfeiffer, K.-L. Kratz, J. Dobaczewski, and P. Möller, *Acta Phys. Pol. B* **27**, 475 (1996).
- [148] B. Pfeiffer, K.-L. Kratz, F.-K. Thielemann, and W. B. Walters, *Nucl. Phys. A* **693**, 282 (2001).
- [149] S. Wanajo and Y. Ishimaru, *Nucl. Phys. A* **777**, 676 (2006).
- [150] Y. Qian and G. Wasserburg, *Phys. Rep.* **442**, 237 (2007).
- [151] K.-L. Kratz, K. Farouqi, and B. Pfeiffer, *Prog. Part. Nucl. Phys.* **59**, 147 (2007).
- [152] S. Nishimura, Z. Li, H. Watanabe, K. Yoshinaga, T. Sumikama, T. Tachibana, K. Yamaguchi, M. Kurata-Nishimura, G. Lorusso, Y. Miyashita, A. Odahara, H. Baba, J. S. Berryman, N. Blasi, A. Bracco, F. Camera, J. Chiba, P. Doornenbal, S. Go, T. Hashimoto, S. Hayakawa, C. Hinke, E. Ideguchi, T. Isobe, Y. Ito, D. G. Jenkins, Y. Kawada, N. Kobayashi, Y. Kondo, R. Kruecken, S. Kubono, T. Nakano, H. J. Ong, S. Ota, Z. Podolyak, H. Sakurai, H. Scheit, K. Steiger, D. Stepenbeck, K. Sugimoto, S. Takano, A. Takashima, K. Tajiri, T. Teranishi, Y. Wakabayashi, P. M. Walker, O. Wieland, and H. Yamaguchi, *Phys. Rev. Lett.* **106**, 052502 (2011).
- [153] J. K. Hwang, A. V. Ramayya, J. H. Hamilton, J. O. Rasmussen, Y. X. Luo, D. Fong, K. Li, C. Goodin, S. J. Zhu, S. C. Wu, M. A. Stoyer, R. Donangelo, X.-R. Zhu, and H. Sagawa, *Phys. Rev. C* **74**, 017303 (2006).
- [154] H. Mach, M. Moszynski, R. L. Gill, G. Molnár, F. K. Wohn, J. A. Winger, and J. C. Hill, *Phys. Rev. C* **41**, 350 (1990).
- [155] J. Pereira, S. Hennrich, A. Aprahamian, O. Arndt, A. Becerril, T. Elliot, A. Estrade, D. Galaviz, R. Kessler, K.-L. Kratz, G. Lorusso, P. F. Mantica, M. Matos, P. Möller, F. Montes, B. Pfeiffer, H. Schatz, F. Schertz, L. Schnorrenberger, E. Smith, A. Stolz, M. Quinn, W. B. Walters, and A. Wöhr, *Phys. Rev. C* **79**, 035806 (2009).
- [156] J. K. Hwang, A. V. Ramayya, J. H. Hamilton, Y. X. Luo, A. V. Daniel, G. M. Ter-Akopian, J. D. Cole, and S. J. Zhu, *Phys. Rev. C* **73**, 044316 (2006).
- [157] E. Cheifetz, R. C. Jared, S. G. Thompson, and J. B. Wilhelmy, *Phys. Rev. Lett.* **25**, 38 (1970).
- [158] H. Hua, C. Y. Wu, D. Cline, A. B. Hayes, R. Teng, R. M. Clark, P. Fallon, A. Goergen, A. O. Macchiavelli, and K. Vetter, *Phys. Rev. C* **69**, 014317 (2004).
- [159] P. Sarriguren and J. Pereira, *Phys. Rev. C* **81**, 064314 (2010).
- [160] P. Sarriguren, A. Algora, and J. Pereira, *Phys. Rev. C* **89**, 034311 (2014).
- [161] F. Browne, A. M. Bruce, T. Sumikama, I. Nishizuka, S. Nishimura, P. Doornenbal, G. Lorusso, P.-A. Söderström, H. Watanabe, R. Daido, Z. Patel, S. Rice, L. Sinclair, J. Wu, Z. Y. Xu, A. Yagi, H. Baba, N. Chiga, R. Carroll, F. Didierjean, Y. Fang, N. Fukuda, G. Gey, E. Ideguchi, N. Inabe, T. Isobe, D. Kameda, I. Kojouharov, N. Kurz, T. Kubo, S. Lalkovski, Z. Li, R. Lozeva, H. Nishibata, A. Odahara, Z. Podolyak, P. H. Regan, O. J. Roberts, H. Sakurai, H. Schaffner, G. S. Simpson, H. Suzuki, H. Takeda, M. Tanaka, J. Taprogge, V. Werner, and O. Wieland, *Phys. Lett. B* **750**, 448 (2015).
- [162] D. Ni and Z. Ren, *Phys. Rev. C* **89**, 064320 (2014).
- [163] E. Y. Yeoh, S. J. Zhu, J. H. Hamilton, A. V. Ramayya, Y. X. Liu, Y. Sun, J. K. Hwang, S. H. Liu, J. G. Wang, Y. X. Luo, J. O. Rasmussen, I. Y. Lee, H. B. Ding, L. Gu, Q. Xu, and Z. G. Xiao, *Phys. Rev. C* **82**, 027302 (2010).
- [164] K. Li, J. H. Hamilton, A. V. Ramayya, S. J. Zhu, Y. X. Luo, J. K. Hwang, C. Goodin, J. O. Rasmussen, G. M. Ter-Akopian, A. V. Daniel, I. Y. Lee, S. C. Wu, R. Donangelo, J. D. Cole, W. C. Ma, and M. A. Stoyer, *Phys. Rev. C* **78**, 044317 (2008).
- [165] A. Petrovici, K. W. Schmid, and A. Faessler, *J. Phys.: Conf. Ser.* **413**, 012007 (2013).
- [166] P. W. Zhao, Z. P. Li, J. M. Yao, and J. Meng, *Phys. Rev. C* **82**, 054319 (2010).
- [167] M. Wang, G. Audi, A. H. Wapstra, F. G. Kondev, M. MacCormick, X. Xu, and B. Pfeiffer, *Chin. Phys. C* **36**, 1603 (2012).
- [168] S. Raman, C. W. Nestor, and P. Tikkanen, *At. Data Nucl. Data Tables* **78**, 1 (2001).
- [169] L. Chaos-Cador and E. Ley-Koo, *Int. J. Quantum Chem.* **97**, 844 (2004).